AN ABSTRACT OF THE THESIS OF

Kevin Terrence Lewis for the degree of Honors Baccalaureate of Science in Mechanical Engineering presented on May 26, 2009. Title: Phase Separation in Microscale Convective Boiling.

Abstract approved:

James Liburdy

It is hypothesized that extracting the vapor from two-phase flow in a microchannel will result in a lowered pressure drop required to drive the flow. The goal of this thesis is to construct an experimental device that will test this hypothesis by comparing a number of phase separating test conditions to respective control conditions that do not allow for any phase separation.

It was discovered that using a transparent, thin-film heater to boil flow in a microchannel required too much power; the heater designed and built for this purpose was burnt out during testing. Possible reasons for the burnout are discussed. The original test plan was modified to boil the flow prior to the microchannel. The trends found from the new test plan supported the hypothesis. Vapor extraction was related to decreases in the pressure drops; however, vapor extraction rates were measured well below their predicted values. Reasons for the discrepancies are discussed. In conclusion, it was found that vapor extraction does decrease microchannel pressure drops due to decreases in two-phase flow effects.

Key Words: two-phase, separation, boiling, pressure drop, head loss

Corresponding E-mail Address: kevin.t.lewis.11@gmail.com

Phase Separation in Microscale Convective Boiling

by

Kevin Terrence Lewis

A PROJECT

submitted to

Oregon State University

University Honors College

in partial fulfillment of

the requirements for the

degree of

Honors Baccalaureate of Science in Mechanical Engineering (Honors Associate)

Presented June 2nd, 2009

Commencement June 2009

Honors Baccalaureate of Science in Mechanical Engineering project of Kevin Terrence Lewis presented on May 26, 2009.

APPROVED:

Mentor, representing Mechanical Engineering

Committee Member, representing Mechanical Engineering

Committee Member, representing Mechanical Engineering

Department Head, Department of Mechanical Engineering

Dean, University Honors College

I understand that my project will become part of the permanent collection of Oregon State University, University Honors College. My signature below authorizes release of my project to any reader upon request.

Kevin Terrence Lewis, Author

ACKNOWLEGEMENTS

I would like to thank my project mentors Dr. James Liburdy and Dr. Deborah Pence, both of whom spent a great deal of time helping me bring this thesis together.

A special thanks to Dr. Brady Gibbons, Colin Hildebrandt, Victor Calderon and other researchers under of Dr. Gibbons. These individuals spent many hours of their free time helping with the manufacturing process of the microchannel heaters.

Thanks to James Yih and Derek Wilson, the two other members of my Senior Project Team that helped me get the project moving. The countless hours in the lab ensured that we had a final product at the end of winter term for the thesis.

I want to thank David Mandrell for his personal interest in this project, which allowed me to use his resources at ONAMI for cutting our microchannel.

Thank you to all the ME Shop personnel that worked on the heater and silicon dioxide masks.

Finally, I would like to thank my wife, friends, and family for all their help in editing my thesis.

Table of Contents Page

I. LIST OF FIGURES

II. LIST OF TABLES

III. LIST OF APPENDICES

IV. LIST OF APPENDIX FIGURES

V. LIST OF APPENDIX TABLES

This is dedicated to my wife, Katherine.

You have helped make me the person I am today,

and I can’t imagine this having been finished without you.

1) Background and Literature Review

Background

In heat transfer applications, a number of heat transfer related benefits have been found for microscale channel geometries over macroscale geometries. The primary benefits are increases in surface area per unit volume ratios and increased heat transfer coefficients. Other benefits include lower total working fluid volume requirements and lower flow rate requirements. On the downside, the microchannel geometries have greater pressure drops and more complex manufacturing processes.

Two-phase boiling flow has some unique characteristics that benefit thermal management. The primary benefit is a large increase in heat transfer rates due to the boiling process. This translates into needing lower fluid flow rates for the same cooling load. Another significant advantage is that boiling flow has a constant temperature throughout the boiling process. This would eliminate any varying temperature distribution problems observed in earlier research. The major downside is the increase in pumping power required to drive the flow.

Membrane vapor extraction has been commonly used for vacuum membrane distillation. The same process is being pursued in an attempt to lower the pressure drop across a microchannel when it contains two-phase boiling flow. Using the principals of Fick's Law and Darcy's Law, extracted vapor flow rates are determinable based on the pressure drop across the membrane and a mean permeation coefficient.

Single Phase Pressure Drops and Heat Transfer

Pressure drops in internal flow are due to the formation of boundary layers and other viscous fluid interactions with the duct walls. Research has shown that the pressure drop depends on two main factors: the flow regime (laminar vs. turbulent) and the geometry of the duct. These two factors determine the effect wall friction has on the flow, the effect viscous fluid interactions

have on the flow, and ultimately determine the pressure drop across the channel.

The flow regime is determined by the Reynolds number of the flow. The Reynolds number is determined by a ratio of the inertia and viscosity of the flow. The Reynolds number from which the flow is considered to have switched from laminar to turbulent depends strongly on the geometry of the duct. For round pipes, the number is usually considered to be about 2300 (White, 2008). However, it has been stated that this number is different for duct geometries that are not round. This number does, however, provide a basis of judging the flow regime in rectangular ducts given that both are internal flow scenarios. It can then be assumed that the laminar-turbulent transition Reynolds number is less than 2300, and that in order to maintain laminar flow, one needs to establish a Reynolds number well below the 2300 mark, such as a Reynolds number below 1800.

When flow is laminar, one can use an equation to determine the frictional pressure drop through the duct based on the fluid, the duct geometry and the flow rate. The equation now commonly used to calculate laminar flow pressure drops, developed initially by Julius Weisbach, is:

$$\Delta p = f \cdot \frac{L}{D_h} \cdot \frac{1}{2} \rho v^2 \tag{1}$$

where v is velocity, ρ is the density of the fluid, L is the length of the channel, D_h is the hydraulic diameter of the duct, and f is the friction factor that is a function of the Reynolds number, the surface roughness, and the duct shape. Note that the pressure drop, Δp, is in units of pressure, not pressure head for this form of the equation. The pressure head form of the equation can be found in most fluids textbooks (see White, 2008 for an example). The hydraulic diameter, D_h, is defined as:

$$D_h = \frac{4A_c}{P_w} \tag{2}$$

where P_w is the wetted perimeter and A_c is the cross sectional area of the duct. The wetted

perimeter only consists of the sides of the duct that are actually in contact with the fluid. For single phase flow, this should be the perimeter of the duct since the entire duct should be filled with fluid.

The friction factor, *f*, depends on the Reynolds number and a constant that is individual to the duct geometry. Shaw and London (1978) developed a table of values listing the constant *fRe* for a number of different rectangular geometries. Each *fRe* number corresponds with an aspect ratio, α^*, defined as:

$$\alpha^* = \frac{2b}{2a} \tag{3}$$

where *b* is half the height of the duct and *a* is half the width of the duct. Most *fRe* for rectangular ducts can be determined using this table and interpolation or by using the equation provided by Shaw and London:

$$f\,Re = 24[1 - 1.3553\alpha^* + 1.9467\alpha^{*2} - 1.7012\alpha^{*3} + 0.9564\alpha^{*4} - 0.2537a^{*5}] \tag{4}$$

To determine *f* for Equation 1, one divides the constant associated with the particular duct geometry by the Reynolds number of the flow:

$$f = \frac{C}{Re}, \quad C = f\,Re \text{ as determined by Shaw and London} \tag{5}$$

The pressure drop that can be calculated using Equations 1-5 acts as a lower limit to the pressure drop that could occur in convective boiling. The lower limit acts as a check to make sure that the experimental results are reasonable and also gives a starting point for the design of the experimental component.

The benefits of single phase thermal management have been studied in depth since the first study of microchannel thermal management was done by Tuckerman and Pease (1981). Their proposal in the report was that cooling capacities of up to 1000 W/cm^2 would be possible with microchannel thermal management. Qu and Mudawar (2002) followed the study with further research that showed lower fluid temperatures, inside and at the exit of the microchannel, were possible at the expense of supplying greater back pressures. This aligns well with the basic

principles of single phase flow pressure drops. As the back pressure increases, the pressure drop across the channel increases. For the same channel, a higher pressure drop means a greater fluid velocity, which can be seen by the relationship established in Equation 1. The greater flow rates result in larger heat transfer coefficients and faster cooling since there is more fluid to take away the same amount of heat.

Zhang et al. (2000) showed that increasing the power input would decrease the pressure drop across the channel. This is due to the relationship of viscosity to the pressure drop as established in Equation 1 and through the friction factor coefficient, *f*, which is defined for a given flow by the Reynolds number. In most of the studies, uneven heat distribution across the microchannel networks caused uneven expansion of the materials, changes in the electronic behaviors, and mechanical fatigue. By increasing the flow rate, they were able to maintain more constant thermal management across the cooling device, but at the cost of increases to pumping power requirements.

Two-phase Pressure Drops

As mentioned, the primary benefits that can be yielded with boiling flow are constant temperatures and more uniform temperature distributions in cooling devices. When flow begins to boil in a pumping process, it is known that the pressure requirements for the process increase drastically. The pressure requirements increase because the expansion of the liquid into a gas accelerates the less dense mass in the flow direction (Apreotesi, 2007). In order to accelerate this mass, a greater force is needed; that force is supplied by a greater back pressure. The larger back pressure translates directly to larger total pressure drops across the flow section.

There are many difficulties that arise in using two-phase boiling flow in microchannels, and particularly in straight microchannel arrays. Mertz et al. (1996) found fluctuations of the two-phase flow and uneven distribution of the two-phase flow in a series of parallel microchannels. In order to minimize the problems incurred from the parallel network of

channels, the project focused on understanding the dynamics of only one microchannel with the aim to expand upon that later.

Qu and Mudawar (2003) observed similar trends in a later study and identified two sources of two-phase instability: pressure drop oscillations and parallel channel instability. The pressure drop oscillations were observed as periodic large amplitude oscillations that could accidentally result in dry-out, where critical heat flux (CHF) is reached. The parallel channel instability was in line with what Mertz et al. (1996) observed. It also had smaller fluctuations and resulted in CHF conditions less frequently than the pressure drop oscillations. For a single microchannel, the parallel channel instability will not be a problem. The pressure drop oscillations, on the other hand, will have a greater chance of damaging test equipment through dry-out. Steinke and Kandlikar (2004) also observed conditions of dry-out, sometimes in entire channels, when performing investigations on two-phase boiling of water in parallel microchannels. In addition, Steinke and Kandlikar found that flow reversal would occasionally occur in the parallel channel microchannel array. Research by Jiang et al. (2001) with even smaller hydraulic diameter microchannels also observed similar results, with dry-out occurring when the fluid films in the contact line would vaporize and expose the poor-heat conducting vapor to the heat flux from the wall.

This becomes a more prominent problem when the boiling begins in the microchannels because forming bubbles are unable to expand in the radial direction as much as they can in macroscale geometries. The bubble quickly fills the cross section of the microchannel and results in annular or stratified flow, as was demonstrated by flow visualization tests done by Qu and Mudawar (2004). As a result, the majority of the expansion is in the flow direction (Jiang et al. 2001 and Zhang et al. 2002) resulting in appreciable pressure drop increases. In some cases, as demonstrated by Steinke and Kandlikar, the direction of flow would reverse in the parallel microchannel arrays due to the uneven pressure distributions in the arrays. Combined with the already large pressure drops found in microscale geometries, the increases in pressure drops

observed in boiling flow lead to even larger back pressures. The pumping requirements become too large and make microchannel convective boiling heat transfer applications expensive and problematic.

Extracting the vapor from the microchannel as it boils is a new area of interest that may reduce the pressure drop increases found in two-phase flow. The goal would be to keep the pressure at or around the pressure drop for single phase flow. With this in mind, the method of vacuum membrane distillation was researched as a potential method for extracting the vapor phase from the boiling water. Some research into the improved thermal management of such systems has been done by Zhou et al. (2006), where improved fluid temperature and heat sink temperature profiles across microchannel networks were observed.

Diffusion through Porous Medium

Due to the complications two-phase flow exhibits in microchannels, the membrane vapor extraction has been researched over the last few years. Vacuum membrane distillation has frequently been used for the vapor extraction process (Smolders and Franken, 1989; Sarti et al., 1993; Lawson and Lloyd, 1997; Tomaszewska, 1999). Vacuum membrane distillation is based on thermally driven evaporation of water through a hydrophobic porous medium.

The gas transport through a porous membrane is governed by Darcy's Law (Apreotesi, 2007). By using an averaged flow rate across the cross-sectional area through which the vapor passes, the microscale phenomenon in the porous medium are simplified to a macroscale proportion. Apreotesi (2007) showed by a magnitude analysis that the complete form of Darcy's Law is not needed in the flow situations found in membrane vapor extraction, and that a more simplified form can be used. The simplified Darcy's Law is shown below:

$$\dot{m}_{vap} = \Delta P \cdot \frac{A_{cs}}{\nu_{vap}} \cdot \frac{\kappa}{L_{mem}} \tag{6}$$

where ΔP is the pressure drop across the membrane, A_{cs} is the cross-sectional area perpendicular

to the vapor flow direction, L_{mem} is the thickness of the membrane, v_{vap} is the kinematic viscosity of the vapor at the gas temperature, and κ is the permeation coefficient. The value of the permeation coefficient is a function of the membrane and the fluid properties. There are several models for determining the permeation coefficient. One such model is the dusty-gas model as described by Mason and Malinauskas (1983) or Lawson and Lloyd (1997). Empirical models for permeation coefficient have also been determined (Schofield et al., 1987; Smolders and Franken, 1989) that take into account the effects of membrane pore radius, membrane porosity, and tortuosity.

The study by Apreotesi et al. (2007) researched the effects of vapor extraction through porous media. In the study, water was flowed through a branching fractal-like microchannel heat sink where the water was boiled and the vapor extracted through a Teflon membrane that formed one wall of the microchannel heat sink. Results from this study were shown to match well predictions made by the use of Darcy's Law as outlined above. This research was extended by Salakij, et al. (2009) where similar results demonstrated dramatic reductions in pressure drops.

In conclusion, vapor extraction capabilities via vacuum membrane extraction should be well predicted by Darcy's Law as simplified by Apreotesi (2007). Predictions can then be compared to experimental results for single microchannels to try and better understand the dynamics of phase separation in microscale convective boiling. As with the results shown by Salakij, et al. (2009), extracting vapor should have significant results that would indicate decreases in pressure drops with greater vapor extraction and lower vacuum pressures.

2) Project Description

Flow Loop

A major portion of the design of the test setup revolved around the design of the flow loop and the instrumentation. Figure 1 shows the flow loop schematic. The flow originates at a syringe pump that is used to control the volume flow rate of the water. The fluid is then heated by a coil of heater tape that is wrapped around copper tubing. The heat input from the heater tape is controlled by a variac to reach a constant inlet temperature. Flow then enters the first plenum of the test device. Two taps allow for temperature and pressure measurements of the inlet flow at the inlet plenum. The flow is then driven through the microchannel where it can be boiled and separated. The separated vapor phase is pulled through a membrane and into a condenser by a vacuum pump. The condensed vapor is collected and measured to determine the vapor extraction rate, the thermodynamic quality, and to verify the predictions.

The liquid remaining in the channel, along with any vapor not extracted, exits the microchannel into the exit plenum where again there are temperature and pressure measuring instruments. The two-phase mixture is then driven into a flash chamber where the left over vapor is separated via gravity from the liquid phase. The remaining water is then collected and weighed. Conservation of mass calculations will allow for the determination of the vapor lost in the flash chamber and a determination of the overall efficiency of the vapor extraction process with the microchannel boiling. While assembling the flow loop, precautions are taken to ensure that there is no air within the system at any point before the flash chamber. The presence of air could disrupt the pressure measurements and the flow, since it can expand and contract. For the test setup, a differential pressure instrument was used instead of two individual pressure measurements because only the pressure difference was needed.

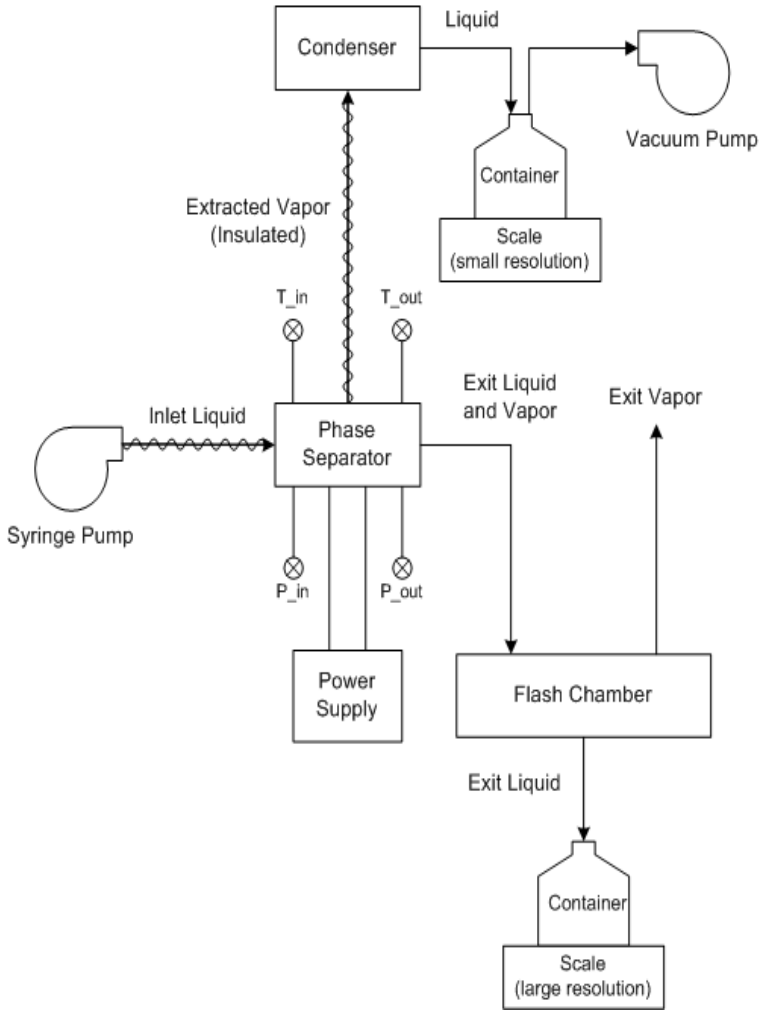

Figure 1: Flow Loop Schematic

Instrumentation

Instrumentation is required for this test in order to verify the hypothesis. Inlet temperature measurements are needed to ensure that the inlet flow is at or near the saturation temperature. The inlet pressure could be estimated by tracking the pressure from the exit into atmospheric pressure back to the inlet plenum, accounting for losses due to entering and exiting the microchannel, losses from exiting the exit plenum, frictional losses in the pipe after the test device, and the pressure increases due to height changes. This could be used in conjunction with the temperature measurement to verify being at or near saturation. The pressure drop is measured with a differential pressure manometer in order to compare vapor extraction and no-vapor

extraction test conditions. The flow rate is determined using a syringe pump. Extracted vapor and exiting liquid masses are caught and weighed separately by individual scales. Below is a list of all the equipment used for testing, the quantity used, and the purpose of the instrumentation.

Table 1: Instrumentation

Equipment	Quantity	Purpose
K-Type Thermocouples	2	Measures the inlet and exit plenum temperatures. A third K-Type was installed, but not used, that could measure the vapor plenum temperature.
Oil Based Differential-Pressure Inclined Manometer	1	Measures the pressure drop from channel inlet to channel exit.
LabVIEW	1	Software that is compatible with the National Instruments equipment used to read the thermocouples.
NI System	1	A Data Acquisition board installed in an NI system was used to measure the voltage across the K-type thermocouples and convert that into a temperature reading within the software.
Syringe Pump	1	Allows the user to set the syringe diameter, flow direction, volume to pump, and volume flow rates. Acted as the principal source of flow rate control.
Vacuum Pump and Gage	1	Air Cadet pump/vacuum that created the vacuum on the porous Teflon membrane. Included in the component was a vacuum gage that was used to determine the vacuum pressure applied.
Small Mass Scale	1	Used to measure the condensed extracted vapor. Resolution to 0.1 mg, maximum weight limit of 80 grams.
Large mass scale	1	Capable of much larger mass measurements than the small mass scale, but resolution only to 0.1 grams. Used to determine the exit mass flow rate.
Olympus Stylus 725 SW Camera	1	Used to take rapid succession pictures of the differential pressure manometer for more accurate determination of pressure drops.

Test Device

The test device for this thesis was fabricated during the winter and spring of 2009. The first attempt at fabricating a working device was during the winter and was conducted by a senior project team at Oregon State University as part of their senior capstone project. The senior project team consisted of James Yih, Derek Wilson, and Kevin Lewis. In the fall of 2008, the

team designed the test device and subsequently built it over the winter term. Following the end of the winter term, the last of the device was completed and assembled for testing.

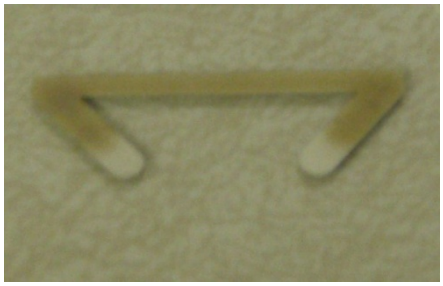

Figure 2: NiChrome heater and SiO_2 base

The device was originally designed to have a clear base for visual confirmation of flow characteristics. This was an important aspect of the design so that further research could be conducted in the future on bubble dynamics of microscale boiling flow with in situ vaporization. The microscale geometry was made out of Kapton (polyimide) and adhered to the clear base. In order to heat the flow through the microchannel, a heater in the form of a thin film of NiChrome (80% Nickel, 20% Chromium) was sputter deposited onto the clear base. The heater was then electrically and chemically isolated from the working fluid with a Silicon Dioxide layer, also sputter deposited. These were both applied prior to the adherence of the polyimide microstructure. An example of the final product for the heater, before applying the polyimide microstructure, is shown in Figure 2. The darker section in the photograph is the insulating SiO_2 cap, underneath which lies a thin layer of NiChrome. The NiChrome can be seen protruding at the end of the leads as the silver-colored part of the device. This exposed NiChrome is used as connection points for the power supply to the heater.

On top of the microchannel is a sheet of Teflon. Two different types of Teflon were used depending on the test. For the experimental conditions, the Teflon sheet used was porous in order to allow for the separation of the vapor from the liquid phase. This Teflon sheet was 150 μm thick with an average pore size of 0.5 μm. The control condition had a non-porous Teflon sheet instead, with a thickness of 127 μm. The goal was to make the two have similar wall conditions for the liquid phase. The chemical make-up of the Teflon is hydrophobic, which helps prevent the liquid water from diffusing through the membrane. The break through pressure for the porous membrane used is around 75-80 kPa pressure difference across the membrane. However, the vapor phase of water is still able to diffuse through the membrane and into the vapor escape

chamber on the other side because of the membranes porosity.

Holding the Teflon to the polyimide is a Nylon block that contains all the test equipment and plenums for the device. The test equipments used to make the necessary temperature and pressure measurements are listed in Table 1 in the Instrumentation section above. In order to ensure that the Teflon was not unnecessarily compressed into the microchannel, shims were used to keep the nylon block a prescribed distance away from the clear base. Vacuum grease was used as a sealant to keep the entire assembly sealed from atmospheric pressure and outside air.

The shims used were 381 μm thick, which match exactly the combined thicknesses of the non-porous Teflon sheet (127 μm) and the polyimide structure (254 μm). However, the porous Teflon sheet at 152 μm thick allows for the porous Teflon to be compressed up to 25 μm into the channel. This should automatically increases the pressure drop across the channel by a small amount. This inherent increase in pressure drop has been calculated using the dimensions mentioned and the testing flow rates used. The increase in pressure from this intrusion in the microchannel should be small, but the increase will be taken into account when comparing the two test conditions.

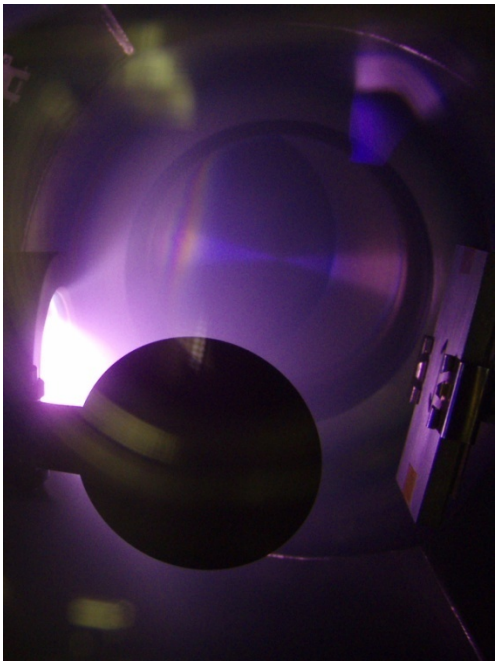

Figure 3: Sputter deposition process

A large portion of the design was focused on the heater used to boil the flow in the microchannel. There were a number of requirements for this heater; the most important requirements were that it had to be transparent and that it had to have a small enough resistance so that the available power supply could be used, in conjuncture with a number of nine volt batteries, to supply enough power to boil the flow. To obtain the transparency needed, the heater was fabricated using a sputter deposition process that created very thin film of metal on the clear

substrate. See Figure 3 for a picture of the sputter deposition process. Shown in the picture is a purple plasma field of SiO_2 (left and center, covered by the dark object) which is being sputter deposited onto the polycarbonate base and mask (right side of picture). The mask ensured that the SiO_2 was only deposited on the desired location of the polycarbonate base. A separate mask was used for the NiChrome sputter deposition, but in a similar manner. NiChrome was used since it demonstrated good resistivity, was easy to obtain, and did not cause any problems during the sputter deposition process. Using the resistivity of NiChrome as reported in prior research by Vinayak et al. (2002), calculations were made so that the sputter deposition times required to produce the desired heater thickness could be predicted from only a few test samples that were deposited on standard laboratory glass slides. The thickness of a heater is inversely proportional to its resistance, and as such it was an important aspect of the design process that the heater remain thin enough to see thought, but also be thick enough that the resistance would not be too high. The larger the resistance, for a set voltage, the less power one can get from the heater; this in concordance with the power law shown in (6). The final heater produced for the project had a resistance of about 6.84 kΩ and was transparent enough to see the flow in the microchannel. The leads to the heater were also sputter deposited, but in order to reduce the resistance of the leads, and thus power lost to the leads, they were sputter deposited to be around seven times thicker than the thin, transparent section on the base of the channel. The sputter deposition for the SiO_2 was much simpler. A short trial and error test with an existing test piece of NiChrome was sputter deposited with SiO_2 until the heater was electrically insulated. The sputter deposition time that was determined from this test was then used to encapsulate the NiChrome heater on the test device.

$$P = \frac{V^2}{R} \tag{7}$$

There were three main aspects to the design of the microchannel: 1) it had to be of microscale, 2) it had to cause the water to boil, and 3) it had to be of an appropriate length that

would produce small, but measurable pressure drops. To satisfy the first condition, the microchannel was given a maximum height of 254 μm. The width of the channel was controlled by the amount of heat necessary to boil the flow. In order to achieve appreciable amounts of heat input, a wider channel of 1500 μm was made to provide more surface area for the heater to cover and thus a lower resistance. The lower resistance meant that a higher heat input could be reached. This was particularly important for the heater design because it allowed for the heater to be thin enough to see through it and still provide sufficient power. If the channel were made thinner, then to obtain the same resistance, a thicker layer of metal would be needed. The length of the microchannel was set to be 20 mm. The pressure drop was part of the reason that this length was chosen, but other factors ended up being more crucial. First, increasing the length would increase the resistance and require a thicker heater or more voltage to maintain good heat input. And second, a longer channel would be more difficult to keep isolated from the air. In satisfying the pressure drop requirement, the length of the microchannel provides small enough pressure drops that they can be measured with a simple inclined differential pressure manometer, but larger flow rates were needed to make sure that the measured pressure drop was large enough that the resolution of the inclined manometer did not create too large an uncertainty. With the inclined manometer used, the resolution was 5 Pa, so in order for this to be a reasonable bias uncertainty, the pressure drop would need to be at least 50 Pa.

The flow parameters for the device consisted of the volume flow rate of the water, the heat input, and the inlet temperature. All three are closely linked and it was important to make decisions for each that allowed for test qualities of low uncertainty, short test times, and ease of reproducibility. No matter what the flow rate, it is best to have the inlet temperature be as close to saturation as possible. However, as the flow rate increases, providing greater pressure drops through the channel, the heat required to bring the water near saturation before the microchannel also increases. In the pursuit of time, appropriate settings for the heater tape were controlled by a variac to obtain near saturation temperatures. This setting was originally determined for a single

flow rate. This fixed both the inlet temperature and the flow rates, so only the heat input was variable. It was this parameter that was varied in the original testing procedures. The final product was intended to produce the situation that can be observed in Figure 4.

Due to complications, the heater design was unable to work properly, partly because of the higher flow rate which was necessary to have low uncertainties. The problems that arose and how they were dealt with are discussed in the Test Plan and Results and Discussion chapters below. As the problems were discovered only after testing was underway, the design of the component was unable to be modified to better fit the new test plan.

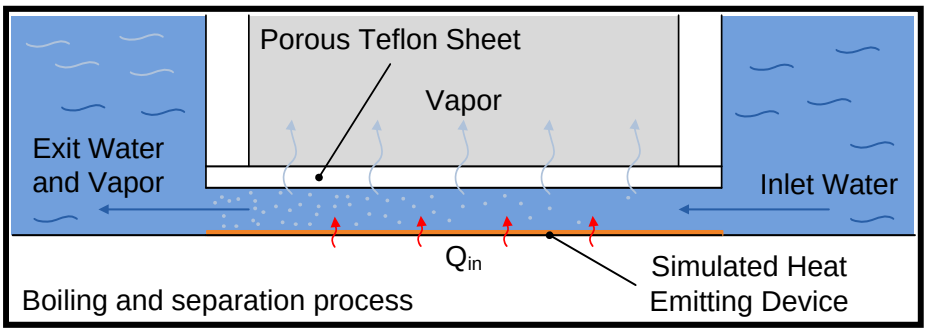

Figure 4: Flow boiling and extraction as original design intended

3) Test Plan

Original Test Plan

Originally, the plan was to test the hypothesis by boiling the flow in the microchannel. This would provide an increase in the pressure drop due to two-phase flow effects in the microchannel. The test would be performed with and without vapor extraction for five different heat input levels from the NiChrome heater at 25, 50, 75, 90, and 100 percent of maximum power. The extracted vapor and exiting water would be weighed to determine the actual thermodynamic quality of water produced, which would be compared to theoretical values that are determined using the laws of conservation of energy and conservation of mass. This test plan would also provide visual insight into the nature of bubble dynamics in two-phase boiling flow with in situ vapor extraction. However, due to complications during testing (see Results and Discussions), the heater was burned out and rendered useless. An alternative test plan was developed in order to continue testing the hypothesis.

Modified Test Plan

The heater tape used to heat the fluid to near saturation prior to the inlet had not yet been maxed out. Therefore, it was used to boil the flow prior to entering the microchannel, in lieu of using the broken microchannel heater. From the inlet plenum, two-phase flow would enter the microchannel and the same phase separation process as mentioned in the design would be used to extract the vapor. The vacuum pressure to pull the vapor through the porous membrane and the inlet volume flow rate was varied to determine their respective effects on the pressure drop and the amount of the vapor extracted.

The first set of tests was run with no vapor extraction to get a basis of comparison for the pressure drop across the channel. The two flow rates used were 3 mL/min and 5 mL/min. The next sets of tests were done with increasing vacuum pressures and constant flow rates. The

vacuum pressure was increased from 10 to 50 kPa in 10 kPa increments during the tests. Pressure drop and vapor extraction data were taken at each vacuum pressure and volume flow rate setting and recorded in a spreadsheet. The test matrices for the experiment, as well as the old test matrices that were going to be used with the NiChrome heater, may be found in Appendix A.

Pressure drop data was collected intermittently throughout a single test period using a camera to capture random measurements of the pressure. Temperature data for the inlet was measured to ensure that the inlet flow was at the saturation temperature and two-phase. The bias uncertainty in the pressure drop is taken from the resolution of the scale. The contributor to the uncertainty in the vapor extracted is the resolution of the scale. In the case of the syringe pump, the uncertainty of the mass flow rate is a combination of the resolution of the syringe pump's step sizes and the density of water. The bias errors, precision errors, and total errors of all measurements can be found in Appendix B.

This test plan was modified again after running the tests. The first tests indicated no measured vapor extraction. In order to ensure that there was vapor extraction, the 3 mL/min tests were rerun for much longer time periods (new: 15 minutes versus old: 3 minutes) and the vacuum tubes were blown out into the collection bottle between tests. This would ensure that all condensed vapor actually made it to the collection bottle. Given time, the 5 mL/min tests should also be rerun to measure their vapor extraction rates.

It is expected that increasing the vacuum pressure will lead to decreases in the pressure drop across the microchannel and increases in the vapor extraction. As such, it is expected that the vapor extraction mass flow rates should be related to decreases in the pressure drop. Finally, it is expected that the vapor extraction mass flow rates follow predictions made using Darcy's Law.

4) Results and Discussion

Problems in Testing

During preliminary testing of the original test plan, it was discovered that the NiChrome heater intended to heat the microchannel could not withstand the necessary voltage to boil the flow. When the full voltage was applied to the heater for a first practice run, the NiChrome heater was burned up or lost in what was assumed to be a hot spot. There are a few reasons that this may have happened. Firstly, the voltage applied to the heater may not have been properly ramped up, and as such, too large of a voltage too quickly could have raised the surface temperature of the heater faster than the water could remove the heat resulting in dry-out at a randomly thin section of the heater. The jump in temperature would have burnt the heater. Secondly, the amount of heat required to boil the flow may not have been a reasonable demand on such a thin heater. It was calculated for the original test plan that a minimum of about 1.04 Watts of power would be needed to raise the temperature of the fluid to saturation from the subcooled temperature of about 96 degrees Celsius. Although this should not be beyond the capacity of the heater if properly cooled, which is in essence the goal of the tests, small fluctuations in the flow would be very dangerous to maintaining a constant temperature across the entire heater. If the distribution were to grow uneven, it would again lead to dry-out and burn the heater. Lastly, the surface that the heater was applied to may not have been properly cleaned before the sputter deposition process. This may have left oils or some other residue on the surface of the polycarbonate base, which may have led to the heater lifting off when the power was applied to it. Whatever the cause, the heater was not handled carefully enough and subsequently broke during testing, so a new method for testing the hypothesis was required, and was developed as outlined in the Test Plan chapter.

To begin the testing, the non-porous Teflon sheet was installed into the test equipment and the no extraction conditions for the 3 mL/min and 5 mL/min flow rates were established. The

Teflon sheet was then swapped out with the porous Teflon sheet and the remaining tests were completed. After the 3 mL/min test run, it was noticed that all the pressure drops appeared to be higher than for the non-porous Teflon test. In trying to establish why this might happen, the 5 mL/min test was started with a test condition of no vapor extraction. It was determined that this pressure drop without extraction was actually higher than when the non-porous Teflon was used. A graph of the two data points and their uncertainties are shown in Figure 5. Here it is clear that there was an increase in the pressure drop when using the porous membrane. Note that the uncertainties are determined with 95% confidence, as are all other uncertainties reported.

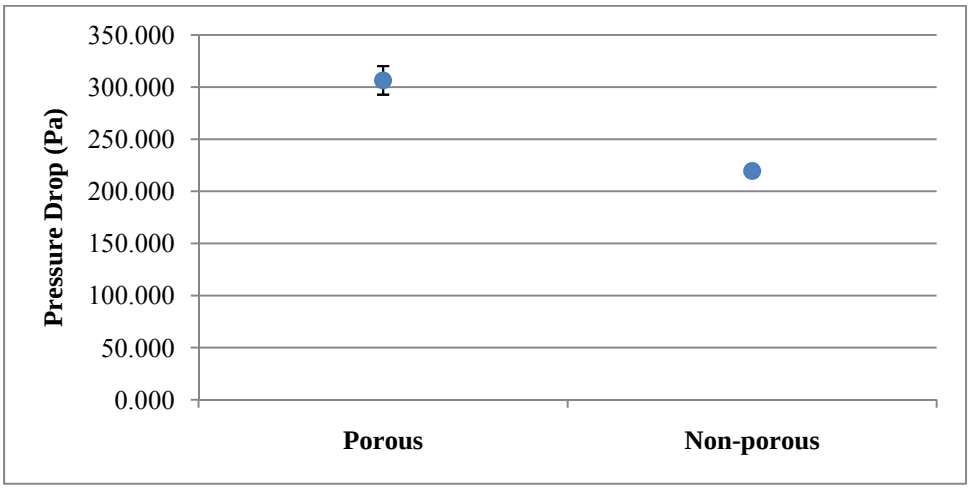

Figure 5: Pressure drops for 5 mL/min flow rate, no vacuum, porous and non-porous Teflon

The 3 mL/min test was run a second time to determine if a similar result was found in that case. Figure 6 depicts the comparison between the 3 mL/min tests with and without the porous Teflon and, as can be seen, a similar trend was observed.

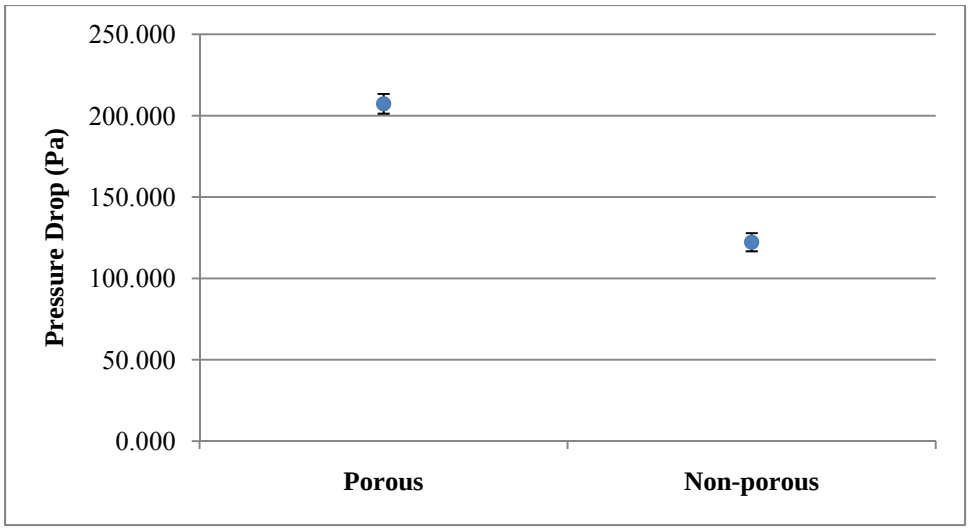

Figure 6: Pressure drops for 3 mL/min flow rate, no vacuum, porous and non-porous Teflon

There are a few reasons why the change in the membrane may have increased the pressure drop. First, the increase in pressure drop may be due to the porous Teflon being thicker than the non-porous Teflon, as mentioned in the chapter on the design of the test equipment. The 10% decrease in cross sectional area at the inlet and exit could be the source for such an increase in pressure drop. This decrease in cross sectional area affects many aspects of the flow. Using the single phase flow equation as outlined in Equation 1 as a model for ratios, with the knowledge that it may be underestimating the rise in pressure drop, a prediction can be made of the increase in pressure drop in a the two-phase flow regime with the change in cross sectional area. By changing the height of the channel the area, perimeter, hydraulic diameter, aspect ratio, and *fRe* number all change. Calculating percentage change in a single phase flow from a blocked to an unblocked channel, the ratio can be applied to the current scenario. For a 30% decrease in cross sectional area, assuming a linear decrease in height with no change in width, that the porous Teflon is at maximum tolerance, and that the channel is not compressed any more than by having the Teflon pressed into the channel, one yields a percentage change in pressure drop of about 280%. The pressure drop has obviously not increase this much, however this calculation was for the extreme condition. In order to raise the non-porous Teflon pressure drop to that of the porous Teflon for the 5 mL/min flow rate test, the membrane need only reduce the cross sectional area by

10%. In the case of the 3 mL/min test, only about a 16% decrease in cross sectional area is needed to do the same. Considering the tolerance on the membrane thickness, both these values are entirely plausible. The difference in channel intrusion may be attributed to different assembly tightness of the test section. Between the two cases, the assembly was opened in order to remove an object from the inlet plenum. During reassembly, the membrane may have been pressed further into the channel and increased the pressure drop further. Figure 7 shows predicted and measured channel pressure drops for the 3 mL/min and 5 mL/min flow rates with the porous Teflon membrane intruding 10% into the channel in both cases. The predictions are made from the non-porous data as mentioned above.

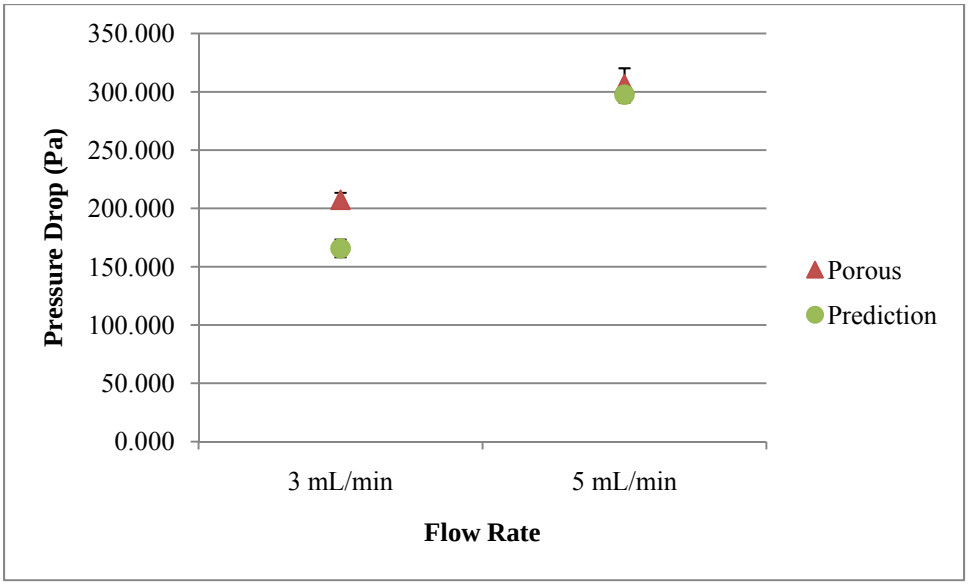

Figure 7: 10% channel reduction, predicted pressure drop increases

At the same time, the non-porous and porous Teflon, being hydrophobic, likely provided surfaces that would not have had the theoretical no-slip relationship with the wall. Trethway and Meinhart (2002) have shown that the hydrophobic character of a solid wall does cause slip with apparent speeds of up to 10% of the free stream velocity, but this was for microchannels on a much smaller scale. It has also been established by Beavers and Joseph (1967), Saffman (1971), and again by Chellam, Weisner, and Dawson (1992) that porous mediums also cause slip conditions due to wall permeability. Although these two conditions would not have increased the

pressure drop, they will have affected the flow. As such, it cannot be determined just how far into the channel the membrane was compressed.

It has been made apparent that the non-porous Teflon test condition cannot be used as a no-vapor extraction control condition since no correction factor can be definitively determined. The best substitute is to have a porous Teflon test condition at zero vacuum pressure. As such, the data point taken for 5 mL/min flow rate and no vacuum pressure with the porous Teflon was used instead of the non-porous Teflon data point. As mentioned earlier, in the case of the 3 mL/min flow rate data, the non-porous Teflon sheet data was disregarded and a new data point with the porous Teflon was taken to verify that the same thing would happen in each case.

Test Results – Pressure Drop

The following are two graphs of pressure drop measurements as compared to the vacuum pressure applied to the membrane, one of each flow rate. The dotted lines on the graphs are not data; they are depictions of the general trends observed in the data. The error bars were obtained from the calculated uncertainty of the mean of the data with ninety-five percent confidence that the true mean falls within the error range shown.

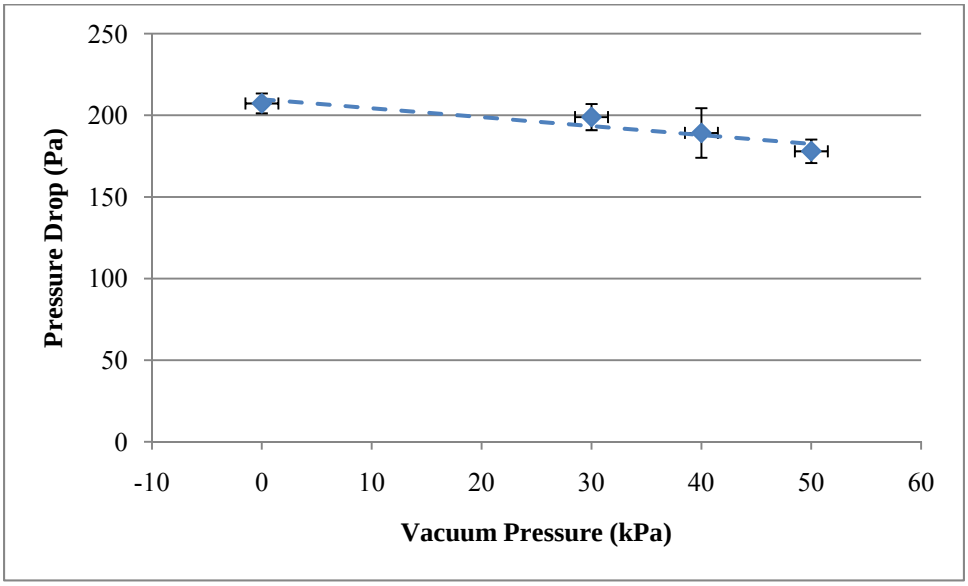

Figure 8: Pressure drop versus vacuum pressure, Flow rate of 3 mL/min

The general trend observed for the 3 mL/min scenario was for the pressure drop across the channel to decrease with increasing vacuum pressure. This agrees well with what was expected from the tests. The uncertainties for the pressure drop are small enough that the trend can be trusted as indicating a true decrease in pressure drop with increases in vacuum pressure. At the very least, it can be said with 95% confidence that the pressure drop across the channel decreases when a 50 kPa vacuum pressure is applied to the backside of the Teflon membrane, since the uncertainties of the 50 kPa vacuum pressure and the 0 kPa vacuum pressure tests don't overlap.

It should be noted that only vacuum pressures of 50 kPa, 40 kPa, 30 kPa, and 0 kPa were used on the 3 mL/min test data. The reason for this is that it was established during testing that vapor extraction was non-measurable at any pressure lower 30 kPa vacuum. This was the second run of the 3 mL/min tests since it was now desirable to attain a no vacuum pressure data point and the modified test plan had not yet included this test run.

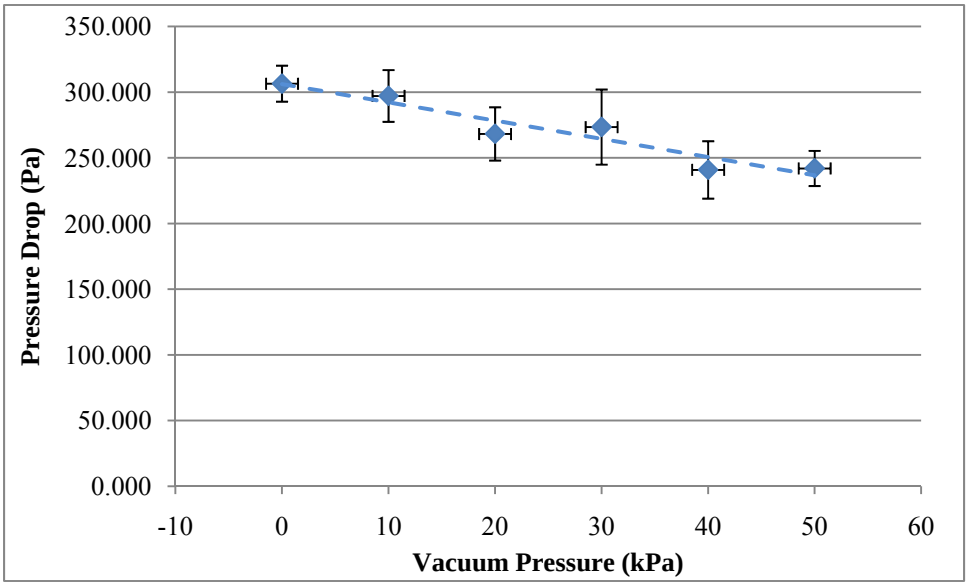

Figure 9: Pressure drop versus vacuum pressure, Flow rate of 5 mL/min

Figure 9 shows a similar trend for the 5 mL/min flow rate tests. As the vacuum pressure increased, the measured pressure drop had the trend to decrease, presumably due to the decrease in two-phase flow effects in the microchannel.

Using the single phase flow model again, it can be shown that the pressure drop across a duct is proportionally related to the flow rate through the duct. As such, a decrease in the flow rate through the duct would result in a proportional decrease of the pressure drop across it. When the largest vacuum pressure for the 3 mL/min flow rate test, 50 kPa vacuum, manages to extract vapor (discussed in the next section), a pressure drop decrease that is solely dependent on the decrease in volume flow rate through the channel can be predicted. Collected vapor extraction and inlet mass flow rate data indicates that 1.16 % of the flow was extracted during the test 50 kPa test. Using the single-phase flow model mentioned earlier, the decrease in flow would yield a proportional decrease in pressure drop of 1.16%. However, it was observed that this extraction actually produced a pressure drop decrease of 14.1%. This would indicate that the pressure drop decreases in the microchannel are not due to decreases in flow rate but, more likely, decreases in two-phase flow effects within the microchannel.

Note that the vertical axes for Figures 7 and 8 intercept the horizontal axes at -10 kPa. This was done so that the graphs would be more readable.

Test Results – Extracted Vapor

There initially appeared to be no measurable vapor extraction for either flow rate at any of the vacuum pressures. The condensed vapor collection bottle was disconnected from the loop after each test segment and weighed to determine if there had been any change in mass, as per the test plan. However, the mass remained constant at all of the vacuum pressure test conditions during the first set of 3 mL/min tests. When the 5 mL/min flow rate tests were started with the 10 kPa vacuum pressure, 337 milligrams of water were suddenly collected in the vapor collection bottle. However, the subsequent tests at 20 kPa and higher did not continue to increase the mass

in the bottle, but decreased it. When all the tests were completed and the condenser emptied, condensate was found all along the condenser tubing immersed in the ice bath. The condensate indicated that there was vapor extraction but that the condensed vapor could not make it to the collection bottle. It is then assumed that the 337 milligrams of water collected at the beginning of the 5 mL/min flow rate tests was left over from the 3 mL/min tests and did not belong to the 5 mL/min flow rate test.

This problem was corrected for during a second set of 3 mL/min tests that were conducted. The reasons for redoing the 3 mL/min flow rate tests were three-fold. One, there was no data point for a 3 mL/min, no vacuum, and porous Teflon sheet test. It was desired to show that the pressure increased when using a porous Teflon sheet over a non-porous one in order to throw out the non-porous Teflon sheet data as not comparable to the porous Teflon sheet pressure drops. Two, the original tests for the 3 mL/min flow rate showed odd trends that had no real explanation. Some ideas may include leaks, breaking in of the Teflon sheet, and an over compressed system, but regardless, new data was required. Finally, the lack of any measured vapor extraction in the previous two tests required more testing with longer test lengths in order to prove vapor extraction.

Since there was condensate on the condenser tubing after emptying the ice bath and there was enough water in the tubes after the 3 mL/min tests that it was later collected at the beginning of the 5 mL/min tests, there is sufficient evidence to assume that vapor was actually being extracted from the microchannel. The problem is finding a way to ensure that it was collected. The final solution was to run the test for a longer time period and then to blow out the tubes into the mass collection bottle at the end of each test. This proved to be very successful, and vapor was collected at all three of the vacuum pressures in the new 3 mL/min flow rate tests.

It has been assumed that no vapor was collected during the first tests because of two reasons. One, the condensed liquid did not have enough of an incline in the condenser tubes to warrant a gravity fed drip into the collection bottle. Two, there was no established airflow in the

tubes, so there was nothing except gravity to force the droplets into the collection bottle. Blowing down the tubes after the test solved this problem by providing airflow to the tubes. The process involved pulling a vacuum on the tubes and then quickly releasing it. The resulting impulse of airflow would dislodge the droplets from the tubes in the condenser and collect them in the bottle downstream. The blow-down process was repeated for several minutes in an attempt to get as much of the condensed vapor into the bottle as possible.

The bottle was then weighed and compared to its weight before the test to determine how much liquid had been collected. This total mass was divided by the test length to determine an average extraction mass flow rate for the test period. Figure 10 shows the relationship between the extracted mass flow rates and their respective microchannel pressure drops. As can be seen in the graph, there is a trend for the pressure drop to decrease as the extraction mass flow rate increases. In comparison to one another, the pressure drop uncertainties indicate the same trend seen in the vacuum pressure versus pressure drop graph in Figure 8. However, it is more difficult to notice the trend as being as dominant as it was Figure 8. Still, it can be said that the pressure does decrease when moving from the 0 to 50 kPa vacuum conditions with 95% confidence.

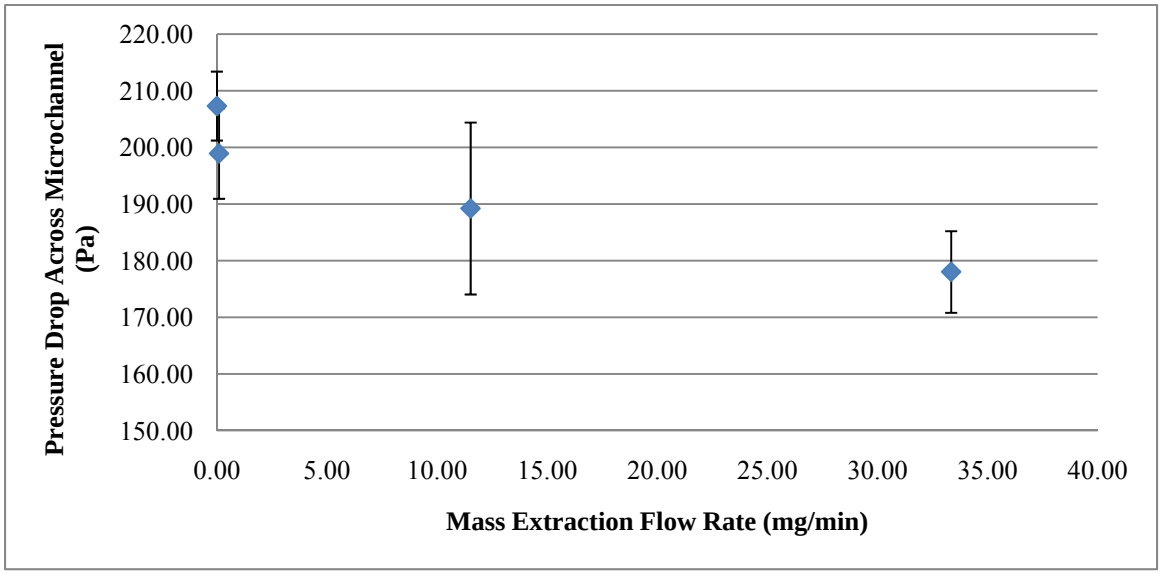

Figure 10: Mass extraction versus Pressure Drop

It is also peculiar how a non linear relationship between vapor extraction and pressure drop is observed. A possible explanation for this trend is that initial, small amounts of vapor extraction led to large changes in the void fraction in the channel, which may in turn resulted in sharper decreases in the pressure drop. Then further increases in mass extraction yielded diminishing returns on pressure drop, which could be due to the void fraction having already been reduced. In order to explore this further, the actual thermodynamic quality or void fraction within the microchannel would be required. A theoretical quality could be determined if at the beginning of every test there was a measurement of collected exiting liquid mass flow rate prior to starting the vacuum pump. This would allow for a mass balance between the inlet and exit flows to determine the amount of mass that was vapor and thus the quality of the flow. This would provide an inlet quality. A mass balance performed with the vapor extraction mass flow rate, exiting liquid mass flow rate, and inlet mass flow rates would allow one to determine the quality of the same test at the exit. However, due to the time sensitive nature of running a test (the syringe pump can only run a specific length of time at any given flow rate before it runs out of water), this additional step was overlooked during testing. Had the measurements been taken, one could use model recommendations from Qu and Mudawar (2003) to predict pressure drop changes in the two-phase flow. The change in quality resulting from vapor extraction would predict changes in the pressure drop due to decreases in two phase boiling flow. To determine theoretical vapor extraction rates for a given vacuum pressure, one would use Darcy's Law. The theoretical change in quality could then be determined and related to a theoretical change in pressure.

If the data were not to follow the two-phase model accurately, another possible explanation for the trend observed could be deformation of the membrane. Applying the vacuum will have put a backward draw on the membrane. If the membrane were not held in enough tension, the tendency would be for the membrane to bow into the vapor plenum. This would effectively increase the cross sectional area of the microchannel and reduce the pressure drop

even if there was no vapor extraction. However, once the membrane had bowed as much as it could, further decreases in pressure drop would require vapor extraction mass flow rate increases. Figure 10 might be demonstrating this by indicating a large pressure drop for relatively little vapor extraction at the lower vacuum pressure (30 kPa). The latter data points, 40 kPa and 50 kPa, indicated significant increases in vapor extraction mass flow rates when, compared to the difference between 0 and 30 kPa, for more gradual decreases in the pressure drop. However, this is purely speculation. In order to support this argument, it would be necessary to take more data points at different vacuum pressures. One would also need to show that the models mentioned earlier did not well predict the pressure drop. If the pressure drop could already be well predicted by the two-phase flow changing-quality models mentioned by Qu and Mudawar (2003), then this explanation is not needed and is false since the data is actually following a quality-pressure drop relationship.

It should also be mentioned that a better method for collecting the vapor may be needed before analyzing either explanation. Figure 10 indicates rather large uncertainties of the pressure and small mass flow rate uncertainties. However, it does not include the bias uncertainty, which cannot be quantified, of the mass extraction rate that exists in not being able to collect all the condensed water. The bias error also exists in the possibility that not all the extracted vapor is condensed. One suggestion would be to have the extraction tube feed into a small cold water bath on a scale. This would instantly condense any vapor that made it through the condenser and would also act as a means to control the evaporation rate. A few simple tests could be run to determine the evaporation rates off of the bath at a number of different vacuum pressures and would allow for the correction of the collected mass based on these measurements. This way any other evaporation in the tubes would remain on the system side and could be collected in the cold water bath after the test. The bath would be held in a closed contained and would have the vacuum applied to the container. The result would be the same vacuum over the entire vapor escape system but with a better control on the collection of the vapor extracted. This may also

increase the extracted vapor mass flow rate data already obtained by ensuring that none of the vapor is lost through the vacuum pump or is unaccounted for by evaporation.

Using Darcy's Law, theoretical extraction mass flow rates were calculated for the 3 mL/min flow rate and compared to the measured flow rates. Figure 11 shows a plot of the actual data as compared to the prediction.

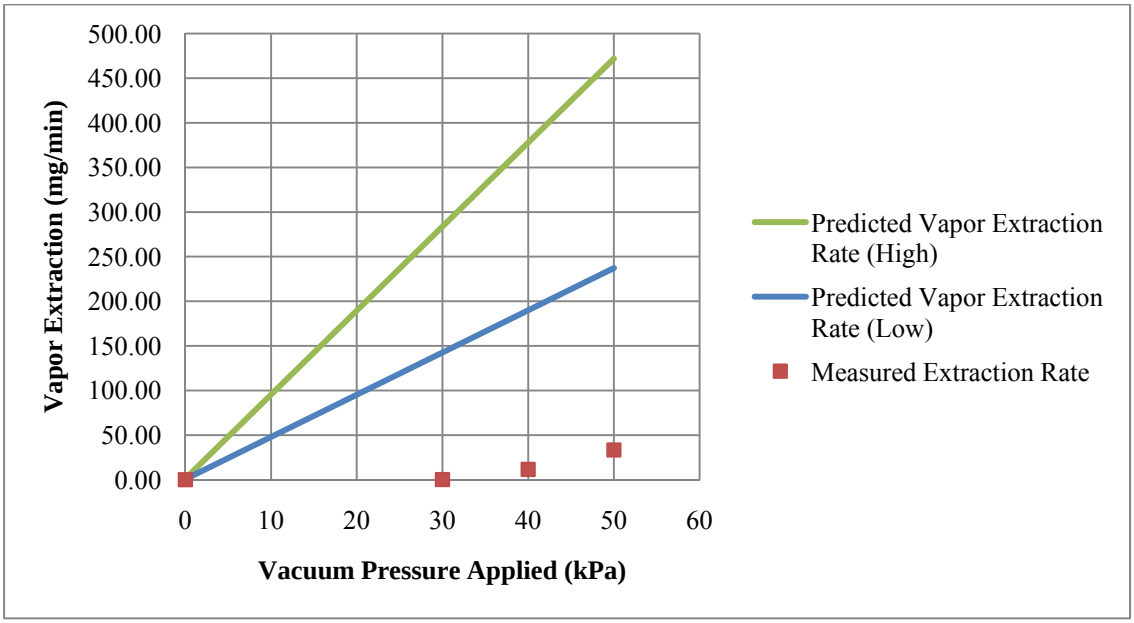

Figure 11: Predicted and actual vapor extraction mass flow rates

As can be seen, the measured vapor extraction falls way below the predicted vapor extraction, about a single order of magnitude lower than the lower prediction. Note that the two different vapor extraction rates, the low and high, are based off the tolerances of the membrane thickness as given by the porous Teflon sheet manufacturer. The good thing is that the data does not exceed the predictions, because that should be possible. Falling below the prediction is entirely possible, and a number of reasons for this happening have been considered. First, the flow was observed to have been in the stratified or wavy flow regime during testing. The test setup had the width of the microchannel in the vertical direction. This may have been the cause of the stratified flow. The stratified flow would effectively reduce the cross sectional area available for vapor extraction, which by Darcy's Law would reduce the vapor extraction mass

flow rate. Secondly, the membrane porosity may have changed due to over compression during the component assembly. Considering the wide range of the membrane's thickness, given as anywhere between 102 μm and 203 μm by the manufacturer, the chance of the shims not being thick enough to prevent compression in to the channel is rather large. Considering the porosity of the membrane, it was not attempted to measure the actual thickness for fear of crushing the pores and preventing vapor extraction. Still, considering that the membrane may have been thicker than expected, given as 123 μm by the distributor, the membrane may have been crushed a little, reducing the porosity of the membrane. If the porosity were decreased by any significant amount, the permeation coefficient would also go down. Darcy's Law would indicate that a decrease in the permeation coefficient would result in a decrease in the vapor extraction mass flow rate. Similarly, if vacuum grease used to seal the component together has been squished into the porous membrane, it may have been pressed into the cross-sectional area over the microchannel. This would again reduce the area available for vapor extraction and once again reduce the vapor extraction rate. Also, not all the extracted vapor was able to be measured due to the complications with condensing and collecting the vapor, so there is a bias error in the uncertainty there that is not known. Lastly, there is about 1-1.5 meters of tubing between the component and the vacuum pump that does not perfectly conduct the vacuum. The gage used to measure the vacuum pressure was installed at the vacuum pump where the vacuum was highest. The actual vacuum applied to the membrane may have been a good deal lower. By Darcy's Law, the decrease in actual vacuum pressure would result in lower predictions that may come closer to the measured vapor extraction rates. Any number of these problems may have contributed to the smaller vapor extraction rates measured.

The same graphs as shown in Figures Figure 10 and Figure 11 are not available for the 5 mL/min flow rate. There was not enough time for the tests to be rerun with the new method used in the 3 mL/min flow rate tests for collecting the condensed vapor. However, it is assumed that the vapor extraction rate results for both cases would be similar. The pressure drop trends of the

3 mL/min and 5 mL/min flow rates are very similar, as is shown in Figures Figure 8 and Figure 9. Extending the similarity allows us to assume that the relationships shown in Figures Figure 10 and Figure 11 for the 3 mL/min flow rate would follow the same trends in the 5 mL/min flow rate tests.

Summary

The data trends indicate that the hypothesis is correct. The trends shown in Figures Figure 8 and Figure 9 indicate that the pressure drop across the channel decreases with increases in vacuum pressure. Figure 11 shows how the vacuum pressure relates to theoretical and actual vapor extraction from the microchannel. The positive relationship established between vacuum pressure and vapor extraction indicates that the pressure drop decreases as vapor extraction mass flow rate in increased, as the trend in Figure 10 appears to indicate.

During testing, many problems arose that necessitated changes in the test plan and the procedure. Given more time, it would be preferable to start testing over again with the knowledge of the problems that were met during the process. The goal would be to produce results that more accurately followed predictions for the vapor extraction mass flow rates. In addition, predictions for pressure drop changes could be made for the two-phase flow. Finally, vapor extraction measurements would be attainable for the 5 mL/min flow rates by following the new procedure used to collect the vapor extracted from the 3 mL/min flow rate tests.

5) Conclusions and Recommendations

As mentioned in the Results and Discussion chapter above, the hypothesis has been supported by the trends observed. Although the data showed trends that supported the hypothesis, there are concerns about the accuracy of the extracted vapor measurements. Areas of interest for further research include: the measurement of inlet and exit qualities for verification of vapor extraction mass flow rates, pursuing the original design intent of boiling flow within a microchannel and observing the changes in pressure observed when extracting the vapor phase produced, and determining better methods to supply a vacuum and still have flow so that the vapor can be transported to a collection bottle or, in the case of a closed loop application, back into the flow loop.

Most obvious in the research is that increases in vacuum pressure reduced the pressure drop across the channel. When comparing solely the mass extraction to the pressure drop, the trend is a little less clear and non-linear. The non-linear relationship may be expected from the effect that quality has on two-phase flow pressure drops, but in order to verify that the data is following this non-linear relationship, inlet and exit quality data is needed. Also, the reduction of two-phase flow effects due to vapor extraction was demonstrated by showing that the reduction in the flow rate through the channel could not be the only source of the change in pressure drop. This was indicated by showing that decreases in flow rates result in linear decreases in pressure drops, and that the measured pressure drop reductions far surpassed the linear reduction that would be predicted using only the decrease in flow rate as justification for the decrease in pressure drop.

This project also stands as a warning to future researchers to use thin film metal heaters very carefully when using them to boil water. The heat required to simply reach saturation from subcooled temperatures of 4-5 degrees still rather large for any kind of appreciable flow rate. Even if a thin film is properly ramped up, pressure drop oscillations and the resulting possibility

of dry-out may cause problems with the reliability of this heating method. It is also extremely difficult to ensure that the film is of an even thickness so that there are no hot spots, which could quickly and easily destroy the heater during testing. Lastly, it is recommended that the surface on which the heater is to be deposited be handled with great care and cleaned thoroughly prior to the heater application. Mishandling the base in these regards may result in damaging the heater or preventing proper application of the heater. It is recommended that if visual confirmation of phase separation in microchannel convective boiling is required, that future researchers pursue an alternate, safer and easier route for boiling the flow. An example would be to heat the fluid via the walls of the channel rather than with a transparent heater along the base. However, one down side to pursuing a side heated channel is that it will not be the same as a base heated scenario which most closely resembles an electronics cooling application. If, however, future researchers were looking to use the same thin heater process, there are a number of recommendations that should be followed. One, use a heater thickness that reduces the impact a hot-spot will have on the testing. It is impossible to ensure a perfect even coat of metal during every sputter deposition, so it is important that this is taken into account when determining the desired thickness. Two, use a variable power supply that can start at a very low voltage. Make sure that the heater output is ramped up very slowly and that the fluid is always cooling the heater. Three, properly clean the surface of the heater substrate prior to the sputter deposition process. Finally, ensure that the inlet water never enters as vapor. The momentary decrease in convective cooling could ruin the heater by causing dry-out.

Lastly, research into methods that can better handle the mass transport of the extracted and condensed vapor would be an important aspect of bringing this technology into real world applications. The vacuum pressure needs to be able to extract the vapor but not pump it into the environment if the system is to be maintained in any kind of a closed loop system that could be used to cool high heat density electronic components. Flow is needed to ensure that the vapor is returned to the system.

Appendix A – Test Matrices

The following are the two test matrices that were intended to be used in the experiment with the NiChrome heater. The first, Table A1, is for the non-porous Teflon sheet and the second, Table A2, is for the porous Teflon sheet. Both matrices have the same test conditions, the only difference being the presence of the porous membrane or the solid membrane. This test plan allows for a comparison of the pressure drop enhancements from using the porous membrane at a number of different qualities and heat inputs. Note that the percent of max power that would be used is the percent of power over the base amount necessary to bring the fluid to saturation. For example, the 0% power case is one in which only enough power is supplied to have the water theoretically reach the saturation temperature and no more. The 25 % case provides one quarter of the remaining power to boil the water.

Table A1: Original non-porous Teflon test matrix

Non-porous Teflon					
Test Number	1	2	3	4	5
Heat Input (in % of Max)	25	50	75	90	100
Heat Input (W)	1.004	2.009	3.013	3.616	4.018
Predicted Quality	7.16E-03	1.43E-02	2.15E-02	2.58E-02	2.87E-02
Vapor Extraction (mg)	NA	NA	NA	NA	NA

Table A2: Original porous Teflon test matrix

Porous Teflon					
Test Number	6	7	8	9	10
Heat Input (in % of Max)	25	50	75	90	100
Heat Input (W)	1.004	2.009	3.013	3.616	4.018
Predicted Quality	7.16E-03	1.43E-02	2.15E-02	2.58E-02	2.87E-02
Vapor Extraction (mg)	534.09	1068.18	1602.27	1922.72	2136.36

The modified test plans used because of the complications are reported below. As mentioned in the Test Plan chapter, the test matrices are a combination of two different flow rates and five different vacuum pressures. In between flow rate tests, it was necessary to refill the syringes, so in the interest of saving time, the vacuum pressure changes were made without

stopping the pump. Each X in the matrices indicates a single test scenario at which both pressure drop measurements and total vapor extracted measurements are made. Each individual test is allowed to run for about 3 minutes to allow enough time for testing all the vacuum pressures at the given inlet flow rate without stopping the syringe pump.

Table A3: Modified non-porous Teflon test matrix

Flow Rate (mL/min)	
3	5
X	X

Table A4: Modified porous Teflon test matrix

		Flow Rate (mL/min)	
		3	5
Vacuum Pressure (kPa Vacuum)	10	X	X
	20	X	X
	30	X	X
	40	X	X
	50	X	X

A small problem arose during these tests; there was no measured vapor extraction. It was found that this was due to the condensed vapor getting stuck in the condenser. A new 3 mL/min flow rate test was run to determine the vapor extraction rates. The test plan was to repeat the old test plan with at least 15 minute test lengths, starting at 50 kPa vacuum pressure and decreasing the vacuum towards zero in 10 kPa increments. When the vacuum pressure no longer appears to extract any vapor over a 15 minute test, the remaining vacuum pressure tests are skipped except for the 0 kPa (i.e. 101 kPa abs.) vacuum pressure scenario which is run to determine a no extraction base for comparison.

Appendix B – Uncertainties

Bias and precision uncertainties were combined using the root-sum-square (RSS) method. The general equation for the RSS method is shown below:

$$u_R = \sqrt{\sum_{i=1}^{n} \frac{\partial R}{\partial x_i} u_{x_i}^2} \tag{8}$$

Where R is the measurement of interest, u_R is the uncertainty in the measurement, n is the number of measurements used to calculate R, x_i is a measurement used to calculate R, and u_{x_i} is the uncertainty in x_i.

Fortunately, the pressure drop uncertainties were only calculated from bias and precision uncertainties, in which case the above equation simplifies to:

$$u_{\Delta P} = \sqrt{{u_{\Delta P_{bias}}}^2 + {u_{\Delta P_{precision}}}^2} \tag{9}$$

Since none of the mass extracted was able to be measured, there was no need to make any calculations in that regard. The following tables contain the bias and calculated precision uncertainties for the pressure drops and the combined total uncertainties for each data point. Final uncertainties were also displayed as error bars on the graphs shown in the Results and Discussion chapter.

Table B1: Uncertainties calculation table, 3 mL/min flow rate

Extraction Pressure (kPa)	Pressure Drop (Pa)	Precision Uncertainty in Pressure (abs. value)	Bias Uncertainty (abs. value)	Total Uncertainty (abs. value)	Total Uncertainty (percent value)
0	207.325	3.503	4.982	6.090	2.9%
30	198.939	6.254	4.982	7.996	4.0%
40	189.225	14.342	4.982	15.183	8.0%
50	178.016	5.202	4.982	7.203	4.0%

Table B2: Uncertainty calculation table, 5 mL/min flow rate

Vacuum Pressure (kPa)	Pressure Drop (in H2O)	Precision Uncertainty in Pressure (abs. value)	Bias Uncertainty (abs. value)	Total Uncertainty (abs. value)	Total Uncertainty (percent value)
0	306.504	12.762	4.982	13.700	4.5%
10	297.163	19.062	4.982	19.702	6.6%
20	268.269	19.650	4.982	20.271	7.6%
30	273.500	28.148	4.982	28.585	10.5%
40	240.869	21.272	4.982	21.847	9.1%
50	241.990	12.420	4.982	13.382	5.5%

The precision uncertainties were calculated using a normal t-distribution statistic for 95% confidence intervals and twenty-nine degrees of freedom (thirty data points). Using t-tables it was determined that the t-statistic value to be used for establishing the uncertainty was 2.045. This number was multiplied by the standard deviation of the mean value for each data set in order to determine the uncertainty of each averaged data point. The standard of the mean value is determined by dividing the standard deviation of the data by the square root of the sample population:

$$\sigma_{mean} = \frac{\sigma_{sample}}{\sqrt{n}} \tag{10}$$

where n is the sample population and σ is the standard deviation.

Table B3: Uncertainty of extraction mass flow rate

Vacuum Pressure	Pressure Drop (Pa)	Pressure Drop Uncertainty (Pa)	Extracted Vapor Mass Flow Rate (g/s)	Extracted Vapor Mass Flow Rate (mg/min)	Vapor Uncertainty (g/s)	Vapor Uncertainty (mg/min)
0	207.33	6.09	0.00E+00	0.00	0.00E+00	0.0000
30	198.94	8.00	1.56E-06	0.09	9.18E-08	0.0055
40	189.22	15.18	1.92E-04	11.52	1.13E-07	0.0068
50	178.02	7.20	5.56E-04	33.35	8.18E-08	0.0049

Table B3 shows the uncertainty table for the extraction mass flow rate of water for the 3 mL/min tests. The uncertainties were determined using the RSS method mentioned at the

beginning of the Appendix. These calculations did require a partial derivative since the flow rate was calculated using the total mass collected and the total time over which it was collected.

Appendix C – Engineering Drawings

The following pages are a collection of all the engineering drawings used over winter and spring of 2009 to build the test component. Two of the drawings are of the NiChrome heater and SiO_2 masks, which are used to fabricate the heater and SiO_2 respectively. The remaining drawings are of actual component that were machined and used as test equipment.

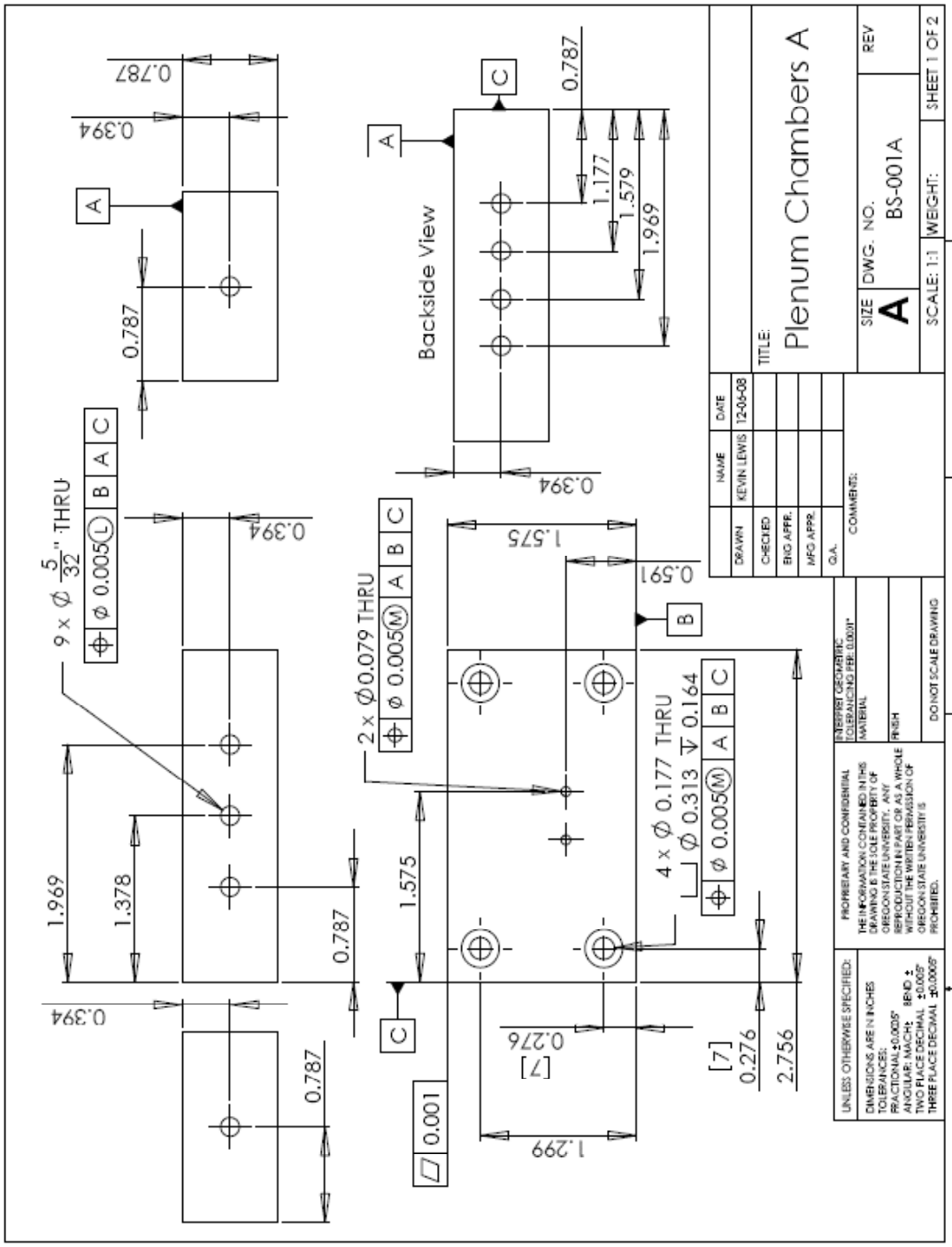
Plenum Chambers A
BS-001A
SIZE A
SCALE: 1:1
WEIGHT:
SHEET 1 OF 2
REV
DWG. NO.
TITLE:
DRAWN
KEVIN LEWIS
12-09-08
CHECKED
ENG APPR.
MFG APPR.
Q.A.
COMMENTS:
NAME
DATE
Backside View
9 x Ø 5/32" THRU
Ø 0.005 L A B C
2 x Ø0.079 THRU
Ø 0.005 M A B C
4 x Ø 0.177 THRU
Ø 0.313 ↧ 0.164
Ø 0.005 M A B C
0.001
1.969
1.378
0.787
0.394
1.575
0.591
1.299
0.276
[7]
2.756
1.177
1.579
1.969
UNLESS OTHERWISE SPECIFIED:
DIMENSIONS ARE IN INCHES
TOLERANCES:
FRACTIONAL ±0.005"
ANGULAR: MACH ± BEND ±
TWO PLACE DECIMAL ±0.005"
THREE PLACE DECIMAL ±0.0005"
PROPRIETARY AND CONFIDENTIAL
THE INFORMATION CONTAINED IN THIS DRAWING IS THE SOLE PROPERTY OF OREGON STATE UNIVERSITY. ANY REPRODUCTION IN PART OR AS A WHOLE WITHOUT THE WRITTEN PERMISSION OF OREGON STATE UNIVERSITY IS PROHIBITED.
INTERPRET GEOMETRIC TOLERANCING PER: ASME Y14.5M
MATERIAL
FINISH
DO NOT SCALE DRAWING

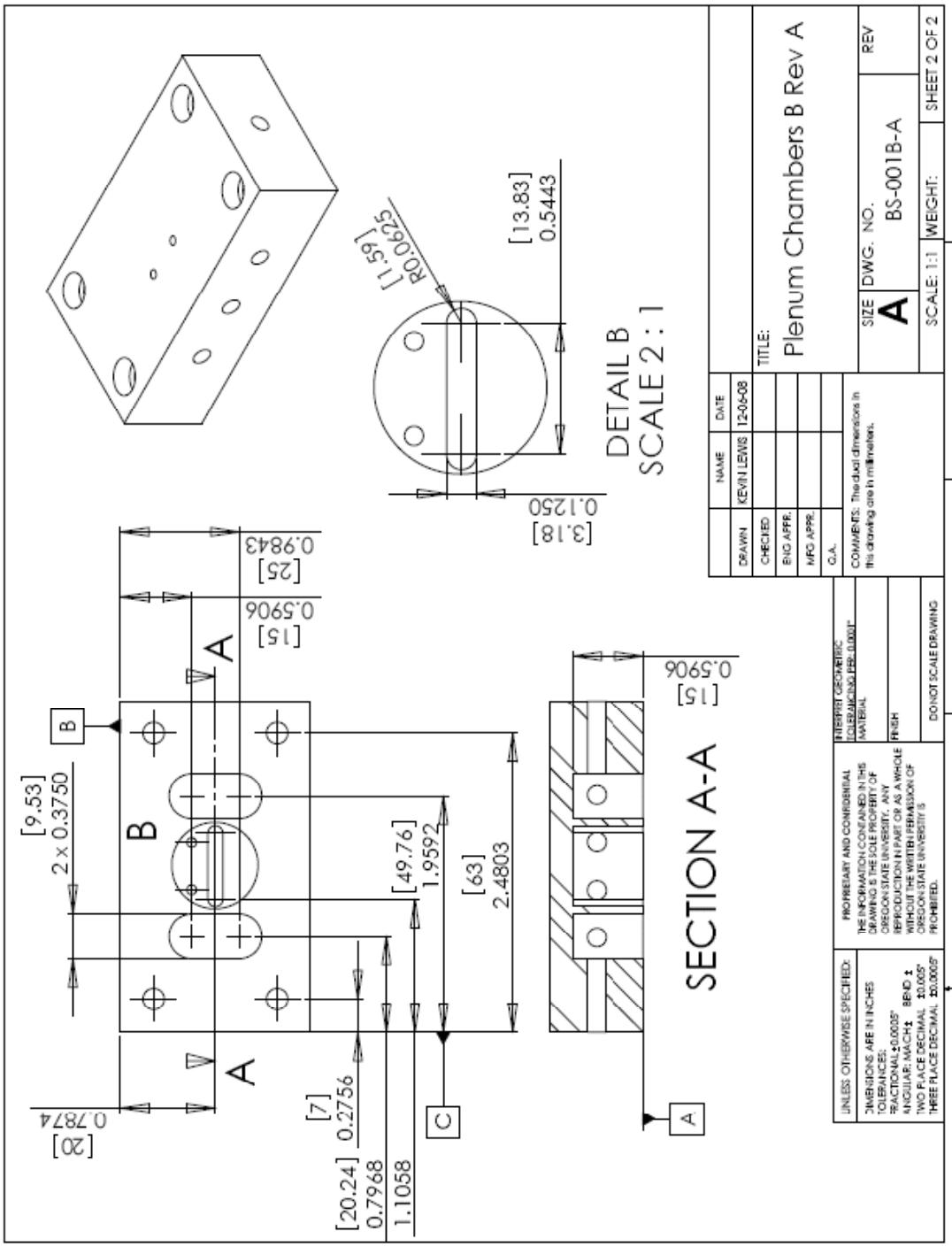
DETAIL B
SCALE 2 : 1
SECTION A-A
Plenum Chambers B Rev A
BS-001B-A
SIZE A
SCALE: 1:1
WEIGHT:
SHEET 2 OF 2
REV
DRAWN
KEVIN LEWIS
12-06-08
CHECKED
ENG APPR.
MFG APPR.
Q.A.
COMMENTS: The dual dimensions in this drawing are in millimeters.
UNLESS OTHERWISE SPECIFIED:
DIMENSIONS ARE IN INCHES
TOLERANCES:
FRACTIONAL ±0.005"
ANGULAR: MACH ± BEND ±
TWO PLACE DECIMAL ±0.005"
THREE PLACE DECIMAL ±0.0005"
PROPRIETARY AND CONFIDENTIAL
THE INFORMATION CONTAINED IN THIS DRAWING IS THE SOLE PROPERTY OF OREGON STATE UNIVERSITY. ANY REPRODUCTION IN PART OR AS A WHOLE WITHOUT THE WRITTEN PERMISSION OF OREGON STATE UNIVERSITY IS PROHIBITED.
FINISH
MATERIAL
INTERPRET GEOMETRIC TOLERANCING PER: ASME Y14.5M-1994
DO NOT SCALE DRAWING
[9.53] 2 x 0.3750
[20] 0.7874
[20.24] 0.7968
[7] 0.2756
1.1058
[49.76] 1.9592
[63] 2.4803
[25] 0.9843
[15] 0.5906
[15] 0.5906
[11.59] R0.4563
[13.83] 0.5443
[3.18] 0.1250

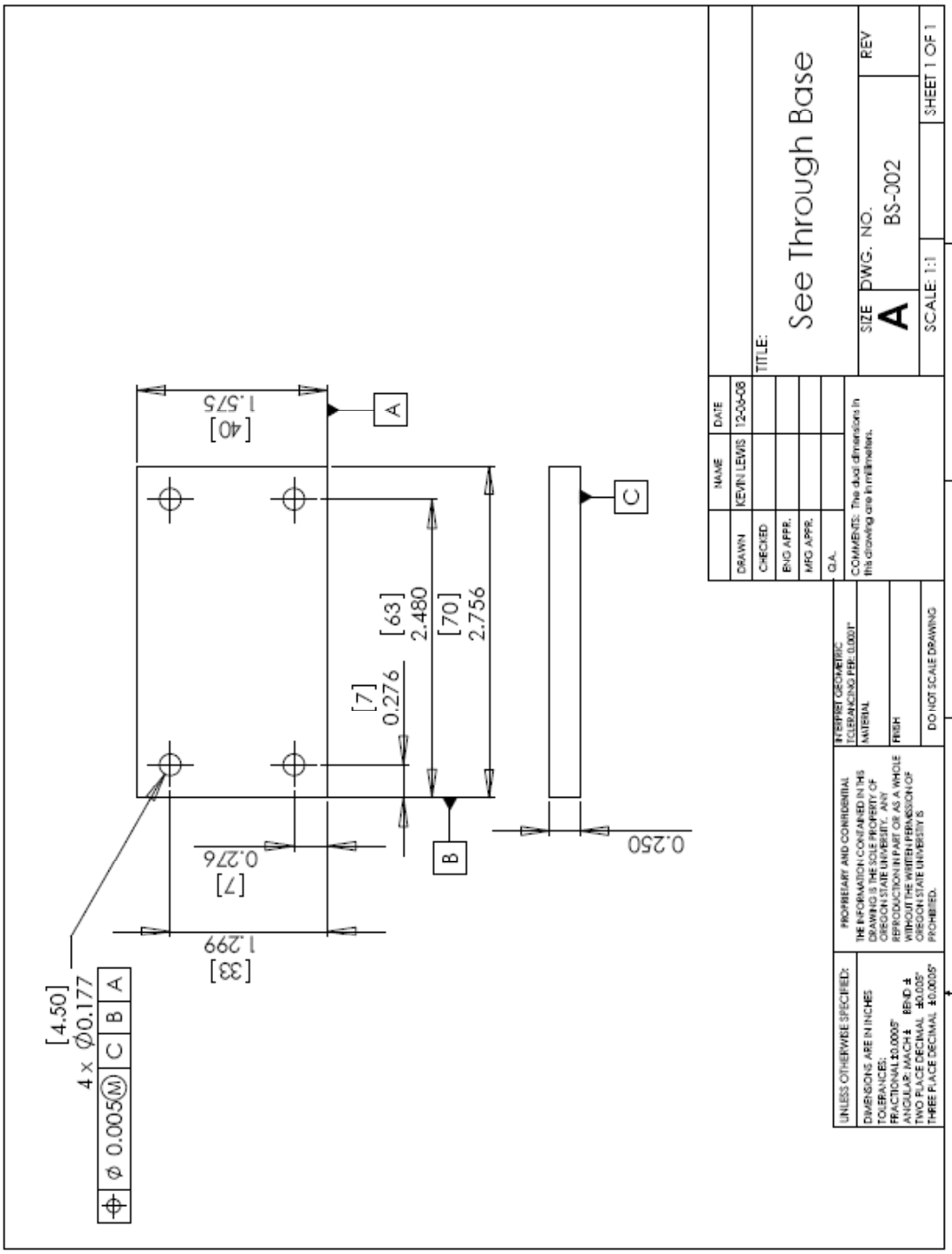
See Through Base
TITLE:
NAME
DATE
DRAWN
KEVIN LEWIS
12-06-08
CHECKED
ENG APPR.
MFG APPR.
Q.A.
COMMENTS: The dual dimensions in this drawing are in millimeters.
SIZE
A
DWG. NO.
BS-002
REV
SCALE: 1:1
SHEET 1 OF 1
UNLESS OTHERWISE SPECIFIED:
DIMENSIONS ARE IN INCHES
TOLERANCES:
FRACTIONAL ±0.0005"
ANGULAR: MACH ± BEND ±
TWO PLACE DECIMAL ±0.005"
THREE PLACE DECIMAL ±0.0005"
PROPRIETARY AND CONFIDENTIAL
THE INFORMATION CONTAINED IN THIS DRAWING IS THE SOLE PROPERTY OF OREGON STATE UNIVERSITY. ANY REPRODUCTION IN PART OR AS A WHOLE WITHOUT THE WRITTEN PERMISSION OF OREGON STATE UNIVERSITY IS PROHIBITED.
INTERPRET GEOMETRIC TOLERANCING PER: ASME Y14.5M-1994
MATERIAL
FINISH
DO NOT SCALE DRAWING
[4.50]
4 × Ø0.177
Ø 0.005 M C B A
[33]
1.299
[7]
0.276
[7]
0.276
[63]
2.480
[70]
2.756
[40]
1.575
0.250
A
B
C

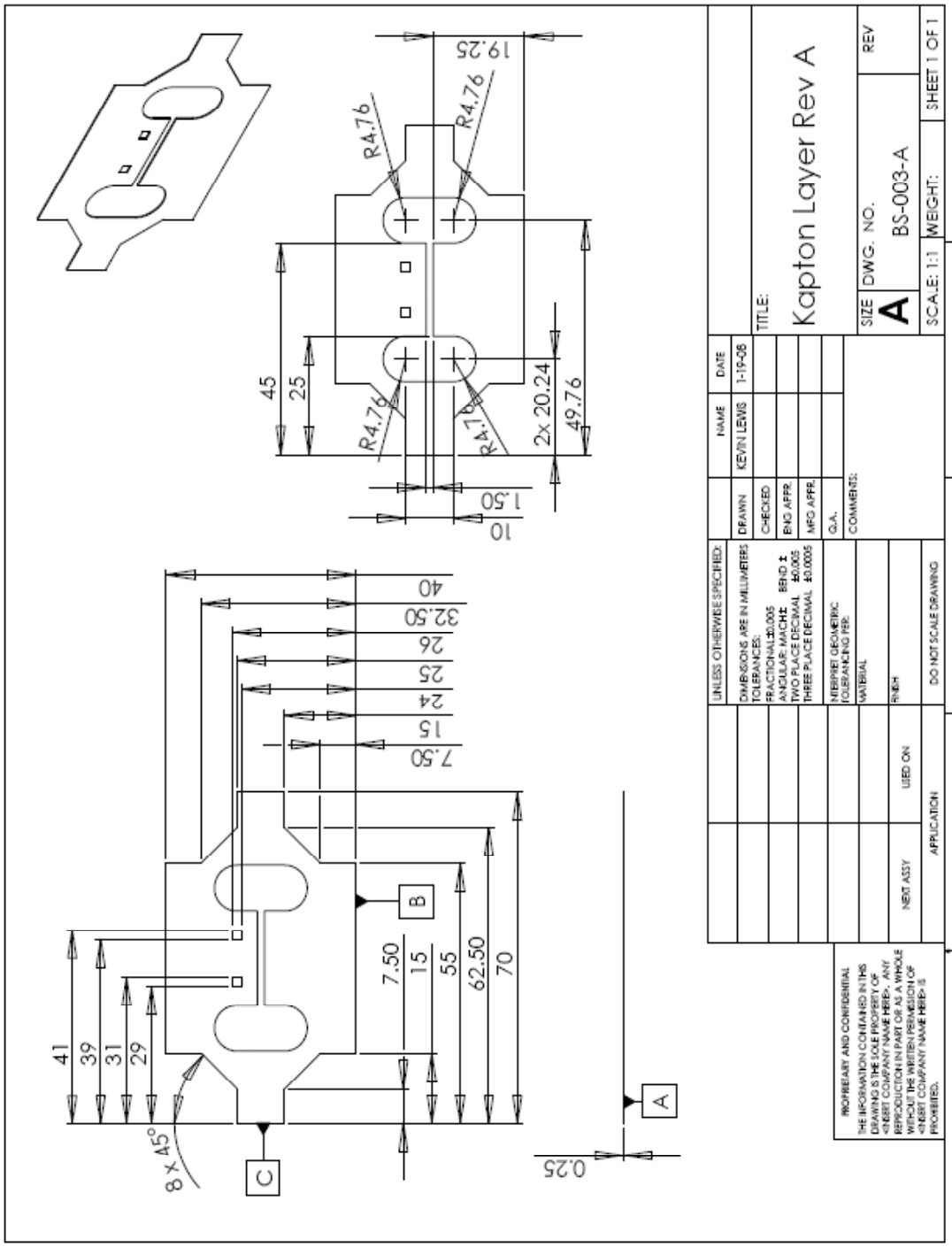
Kapton Layer Rev A
BS-003-A
SIZE A
SCALE: 1:1
WEIGHT:
SHEET 1 OF 1
REV
DRAWN
KEVIN LEWIS
1-19-06
CHECKED
ENG APPR.
MFG APPR.
Q.A.
COMMENTS:
UNLESS OTHERWISE SPECIFIED:
DIMENSIONS ARE IN MILLIMETERS
TOLERANCES:
FRACTIONAL ±0.005
ANGULAR: MACH ± BEND ±
TWO PLACE DECIMAL ±0.005
THREE PLACE DECIMAL ±0.0005
INTERPRET GEOMETRIC TOLERANCING PER:
MATERIAL
FINISH
DO NOT SCALE DRAWING
NEXT ASSY
USED ON
APPLICATION
PROPRIETARY AND CONFIDENTIAL
THE INFORMATION CONTAINED IN THIS DRAWING IS THE SOLE PROPERTY OF <INSERT COMPANY NAME HERE>. ANY REPRODUCTION IN PART OR AS A WHOLE WITHOUT THE WRITTEN PERMISSION OF <INSERT COMPANY NAME HERE> IS PROHIBITED.
19.25
R4.76
R4.76
45
25
R4.76
R4.76
2x 20.24
49.76
10
1.50
40
32.50
26
25
24
15
7.50
41
39
31
29
8 X 45°
7.50
15
55
62.50
70
B
C
A
0.25

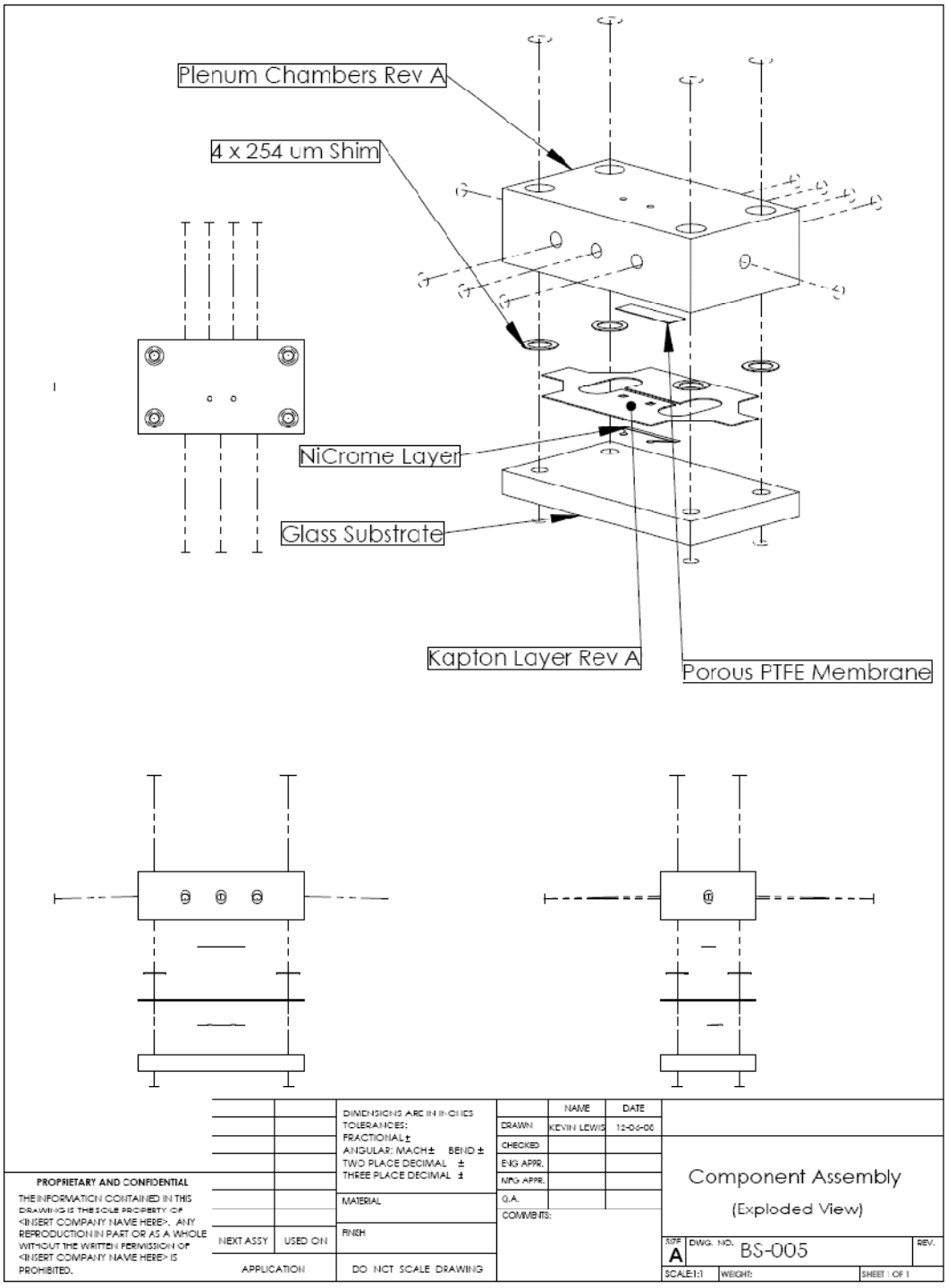

		DIMENSIONS ARE IN INCHES TOLERANCES: FRACTIONAL ± ANGULAR: MACH ± BEND ± TWO PLACE DECIMAL ± THREE PLACE DECIMAL ±		NAME	DATE
			DRAWN	KEVIN LEWIS	12-06-06
			CHECKED		
			ENG APPR.		
			MFG APPR.		
		MATERIAL	Q.A.		
NEXT ASSY	USED ON	FINISH	COMMENTS:		
APPLICATION		DO NOT SCALE DRAWING			

PROPRIETARY AND CONFIDENTIAL

THE INFORMATION CONTAINED IN THIS DRAWING IS THE SOLE PROPERTY OF <INSERT COMPANY NAME HERE>. ANY REPRODUCTION IN PART OR AS A WHOLE WITHOUT THE WRITTEN PERMISSION OF <INSERT COMPANY NAME HERE> IS PROHIBITED.

Component Assembly

(Exploded View)

SIZE	DWG. NO.	REV.
A	BS-005	
SCALE:1:1	WEIGHT:	SHEET 1 OF 1

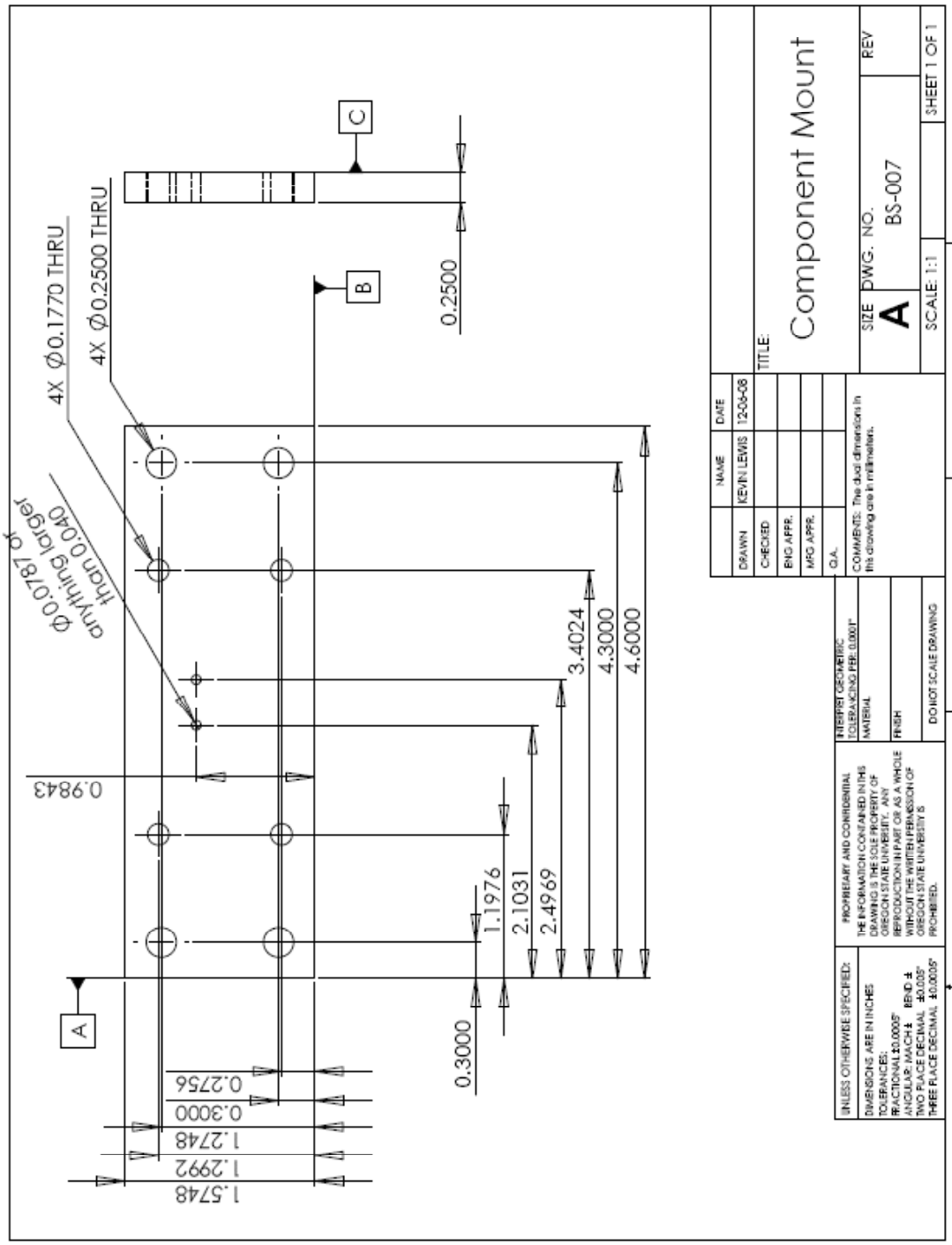
4X Ø0.1770 THRU
4X Ø0.2500 THRU
Ø0.0787 or anything larger than 0.040
0.2500
0.9843
0.3000
1.1976
2.1031
2.4969
3.4024
4.3000
4.6000
0.2756
0.3000
1.2748
1.2992
1.5748
A
B
C
Component Mount
DRAWN
KEVIN LEWIS
12-08-08
CHECKED
ENG APPR.
MFG APPR.
Q.A.
COMMENTS: The dual dimensions in this drawing are in millimeters.
SIZE A
DWG. NO. BS-007
REV
SCALE: 1:1
SHEET 1 OF 1
DO NOT SCALE DRAWING

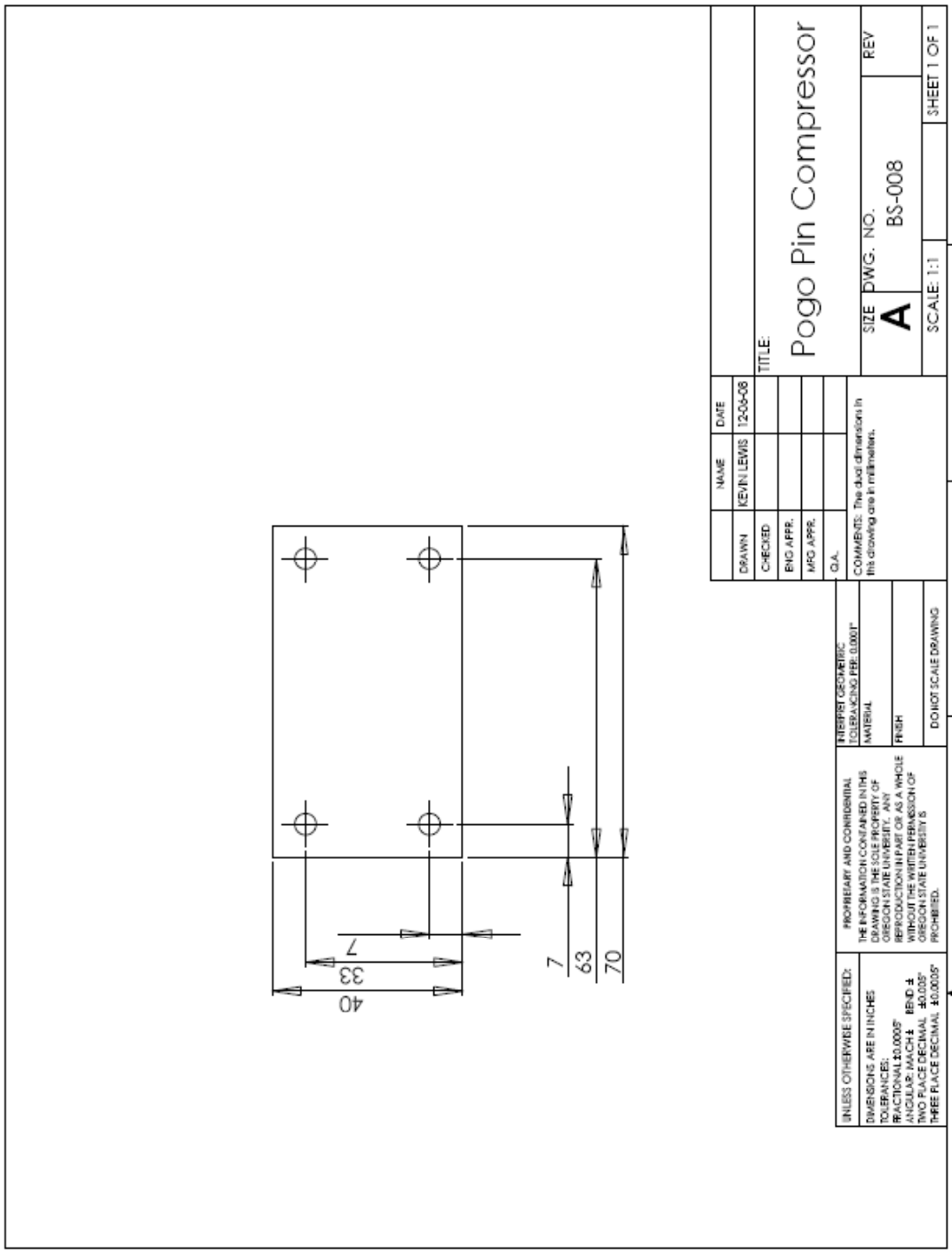
40
33
7
7
63
70
NAME
DATE
DRAWN
KEVIN LEWIS
12-06-08
CHECKED
ENG APPR.
MFG APPR.
Q.A.
TITLE:
Pogo Pin Compressor
SIZE
A
DWG. NO.
BS-008
REV
SCALE: 1:1
SHEET 1 OF 1
UNLESS OTHERWISE SPECIFIED:
DIMENSIONS ARE IN INCHES
TOLERANCES:
FRACTIONAL ±0.0005"
ANGULAR: MACH ± BEND ±
TWO PLACE DECIMAL ±0.005"
THREE PLACE DECIMAL ±0.0005"
PROPRIETARY AND CONFIDENTIAL
THE INFORMATION CONTAINED IN THIS DRAWING IS THE SOLE PROPERTY OF OREGON STATE UNIVERSITY. ANY REPRODUCTION IN PART OR AS A WHOLE WITHOUT THE WRITTEN PERMISSION OF OREGON STATE UNIVERSITY IS PROHIBITED.
INTERPRET GEOMETRIC TOLERANCING PER: ASME Y14.5M-1994
MATERIAL
FINISH
DO NOT SCALE DRAWING
COMMENTS: The dual dimensions in this drawing are in millimeters.

The inside corners do not need to be square, they just need to be as small as can be reasonably achived.

The thinnest the material should be is 0.003" and the thickest it should be is 0.010". Perferably somthing 0.005" thick.

The material should be Aluminum, but the final decision on that has not been finalized.

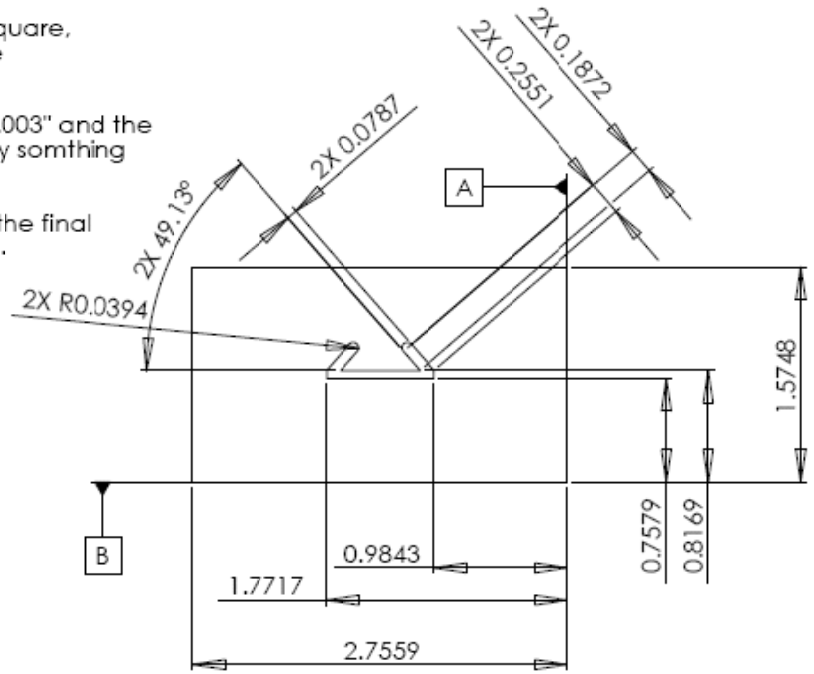

		UNLESS OTHERWISE SPECIFIED:		NAME	DATE
		DIMENSIONS ARE IN INCHES TOLERANCES: FRACTIONAL± ANGULAR: MACH± BEND ± TWO PLACE DECIMAL ±0.0002 THREE PLACE DECIMAL ±0.0002	DRAWN		
			CHECKED		
			ENG APPR.		
			MFG APPR.		
			Q.A.		
		INTERPRET GEOMETRIC TOLERANCING PER:	COMMENTS:		
		MATERIAL Aluminum Note: This is not for certain yet			
NEXT ASSY	USED ON	FINISH			
APPLICATION		DO NOT SCALE DRAWING			

TITLE: NiChrome Mask

SIZE	DWG. NO.	REV
A		
SCALE: 1:1	WEIGHT:	SHEET 1 OF 1

5 4 3 2 1

The inside corners do not need to be square, they just need to be as small as can be reasonably achived.

The thinnest the material should be is 0.003" and the thickest it should be is 0.010". The perfered thickness is 0.005".

The material should be Aluminum, but the final decision on that has not been finalized.

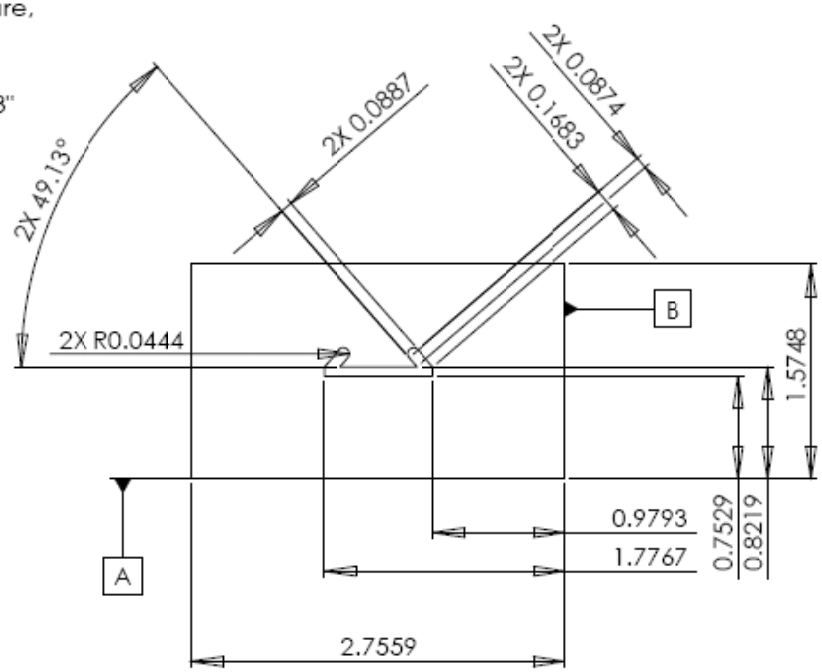

		UNLESS OTHERWISE SPECIFIED:		NAME	DATE
		DIMENSIONS ARE IN INCHES TOLERANCES: FRACTIONAL±	DRAWN		
			CHECKED		
		ANGULAR: MACH± BEND ±	ENG APPR.		
		TWO PLACE DECIMAL ±0.0002 THREE PLACE DECIMAL ±0.0002	MFG APPR.		
			Q.A.		
		INTERPRET GEOMETRIC TOLERANCING PER:	COMMENTS:		
		MATERIAL: Aluminum Note: This is not finalized yet.			
NEXT ASSY	USED ON	FINISH			
APPLICATION		DO NOT SCALE DRAWING			

TITLE: SiO2 Mask

SIZE	DWG. NO.	REV
A		
SCALE: 1:1	WEIGHT:	SHEET 1 OF 1

5 4 3 2 1

Appendix D – Equipment Photos

Included here are a number of pictures of the flow loop, the component, and some example photos of the pressure drops. The pressure drop photos were used to get more accurate readings from the inclined manometer during data collection.

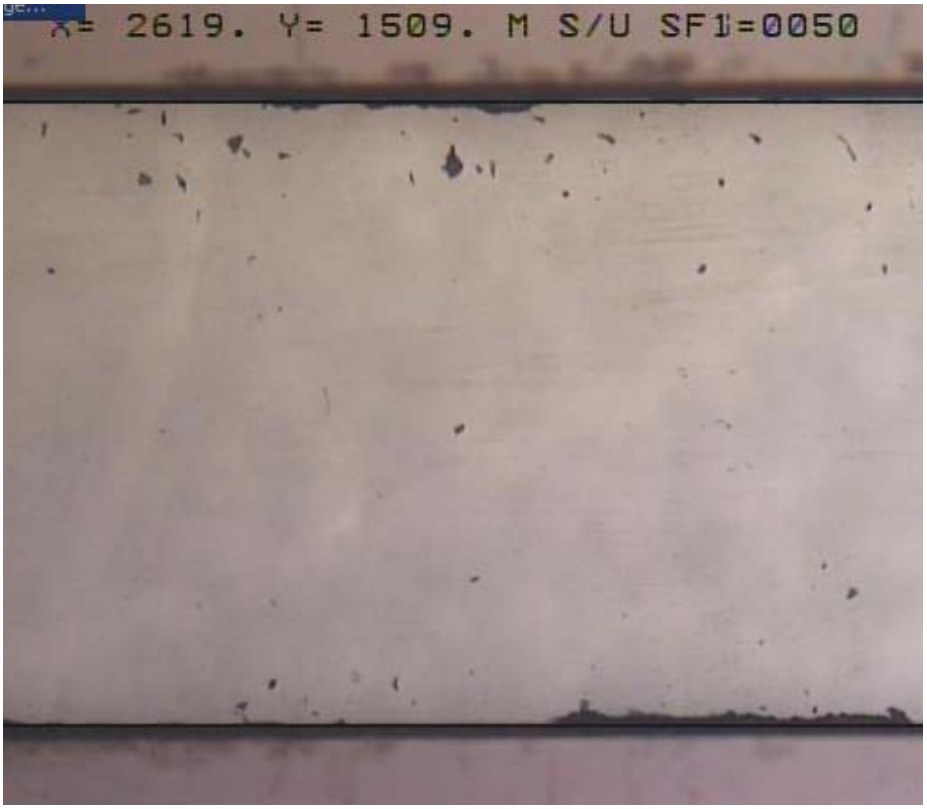

Figure D1: Photo of the laser cut microchannel under a microscope

Figure D1 shows a picture of the microchannel under a microscope. The numbers along the top indicate relative positions of the top and bottom of the microchannel from some datum, measured in micrometers. As can be seen, the channel is exactly 1500 μm wide. The darker material that enters the channel is the adhesive from the back of the polyimide. Besides the small amount of glue that appears to enter the channel, the edge walls of the microchannel are extremely flat with no other visible protrusions. This helps ensure that the flow regime stays laminar and that the microchannel cross sectional area, which directly affects the pressure drop, remains constant along the entire length of the channel.

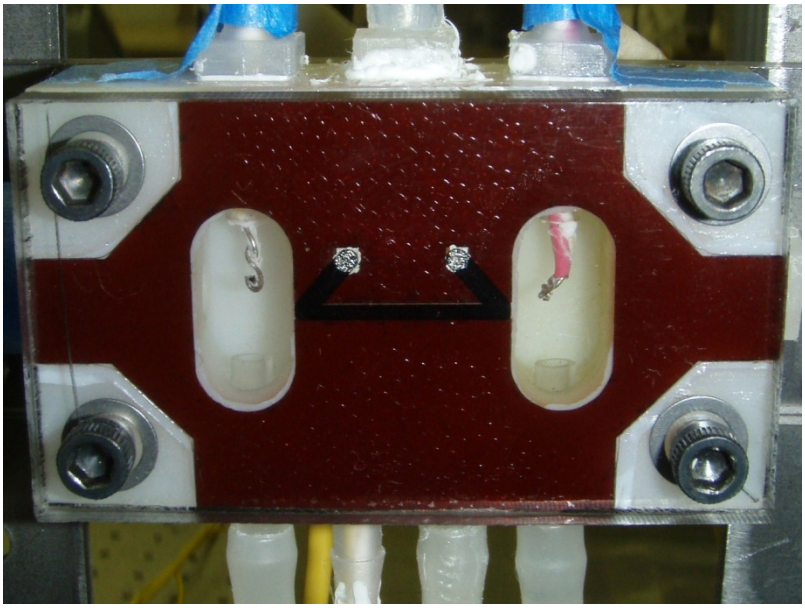

Figure D2: Test setup completely filled with water.

Figure D2 shows the experimental setup as originally designed. The microchannel is currently hidden from view by a heater that was made too thick to see through clearly (although it would still allow visibility with extra lighting). The silver spots were where the heater would be connected to pogo-pins that connected the heater to a circuit. The wires extending into the middle of the plenums are the K-type thermocouples. The holes in the bottom of the plenum are the pressure taps that lead to the inclined manometer not shown in the picture. The flow enters from the right and exits on the left.

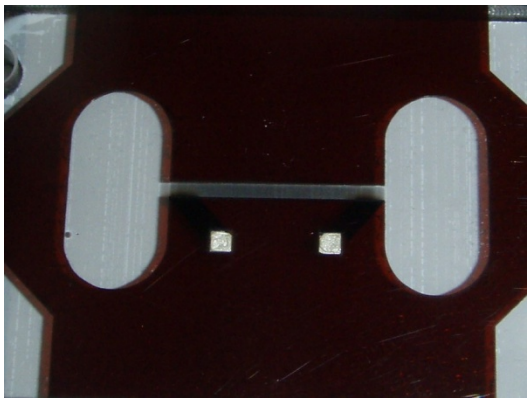

Figure D3: Picture of the transparent heater and microchannel out of the test setup

The picture above shows the heater before it shorted during the testing. Although a little

difficult to see from the picture alone, this heater was transparent and the flow in the microchannel was easily visible. It replaced the thicker heater shown in Figure D2. When the heater shown in Figure D3 shorted, the thicker heater was tried. However, it appears that the thicker heater had some kind of defect because its resistance was measuring around 21 kΩ and a proper connection was sporadic at best.

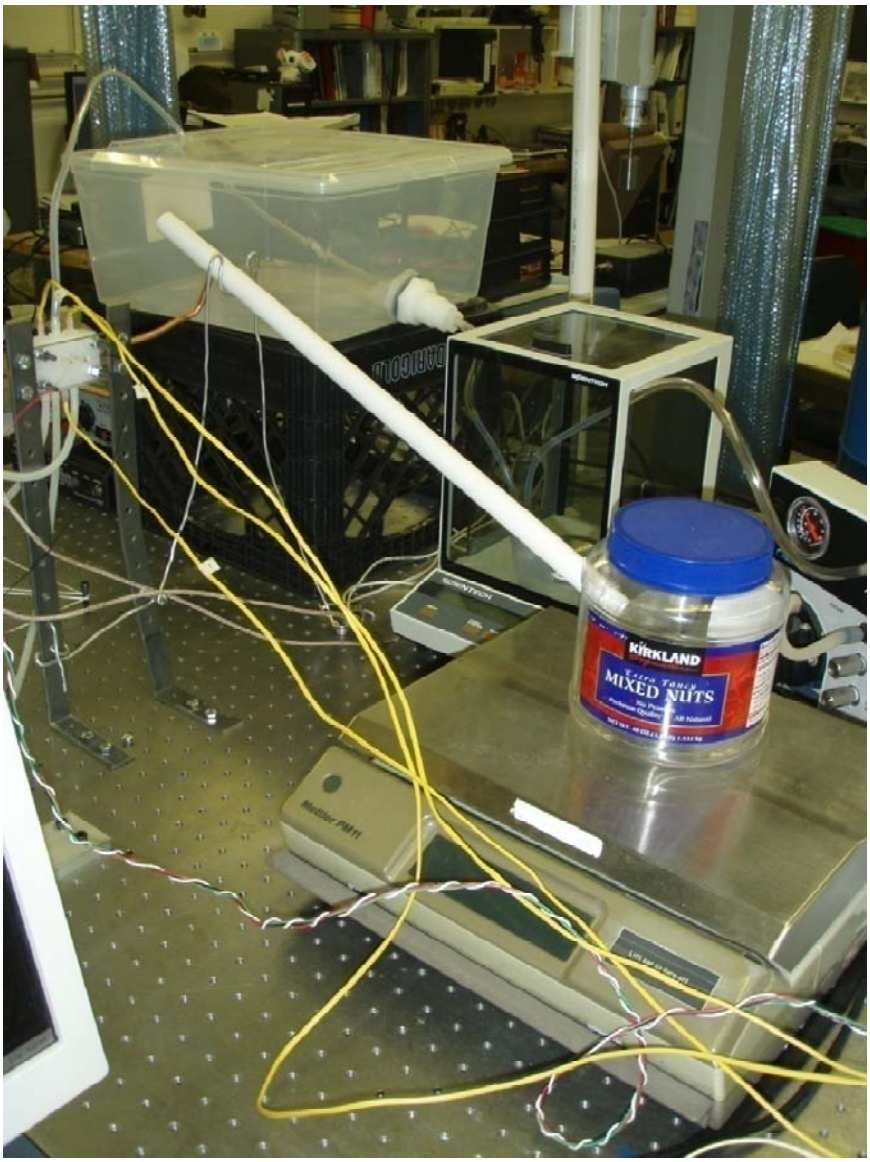

Figure D4: Condenser and mass scales

The picture above shows the large mass measuring scale (front), the small mass measuring scale (back), and the condenser without the ice bath (back left). The yellow wires seen

are the thermocouples leading to the DAQ board not shown on screen. These were moved underneath the mass scale for testing to keep them out of the way. In the end, the larger mass scale was not used due to the change in test plan, which is unfortunate because it may have given data on the quality of the flow.

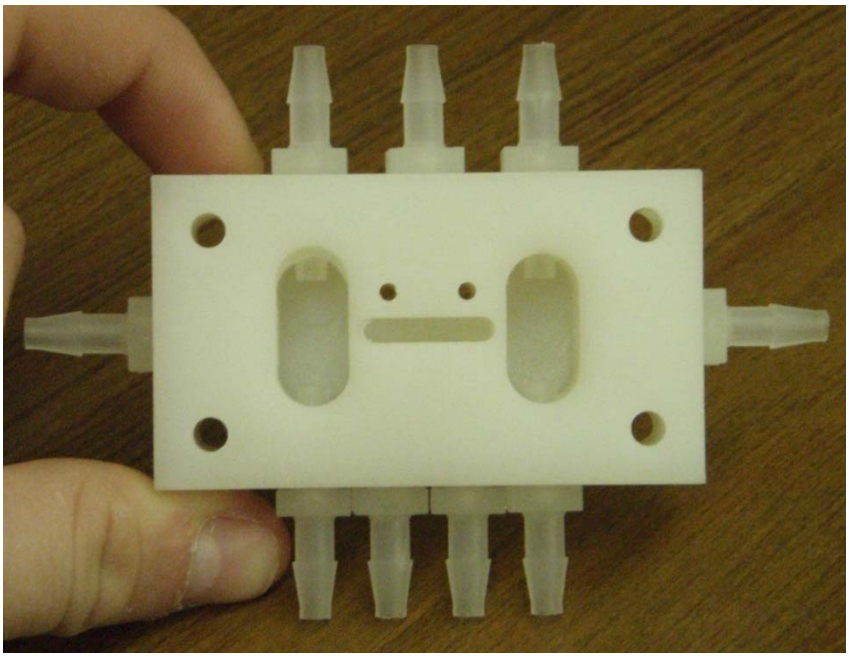

Figure D5: Nylon plenum chambers with instrumentation taps

Figure D5 shows the nylon part made during the winter for the test setup. It contains the inlet and exit flow plenums, the vacuum pulled vapor plenum, the pogo-pin lead holes, and all the holes necessary for instrumentation and flow.

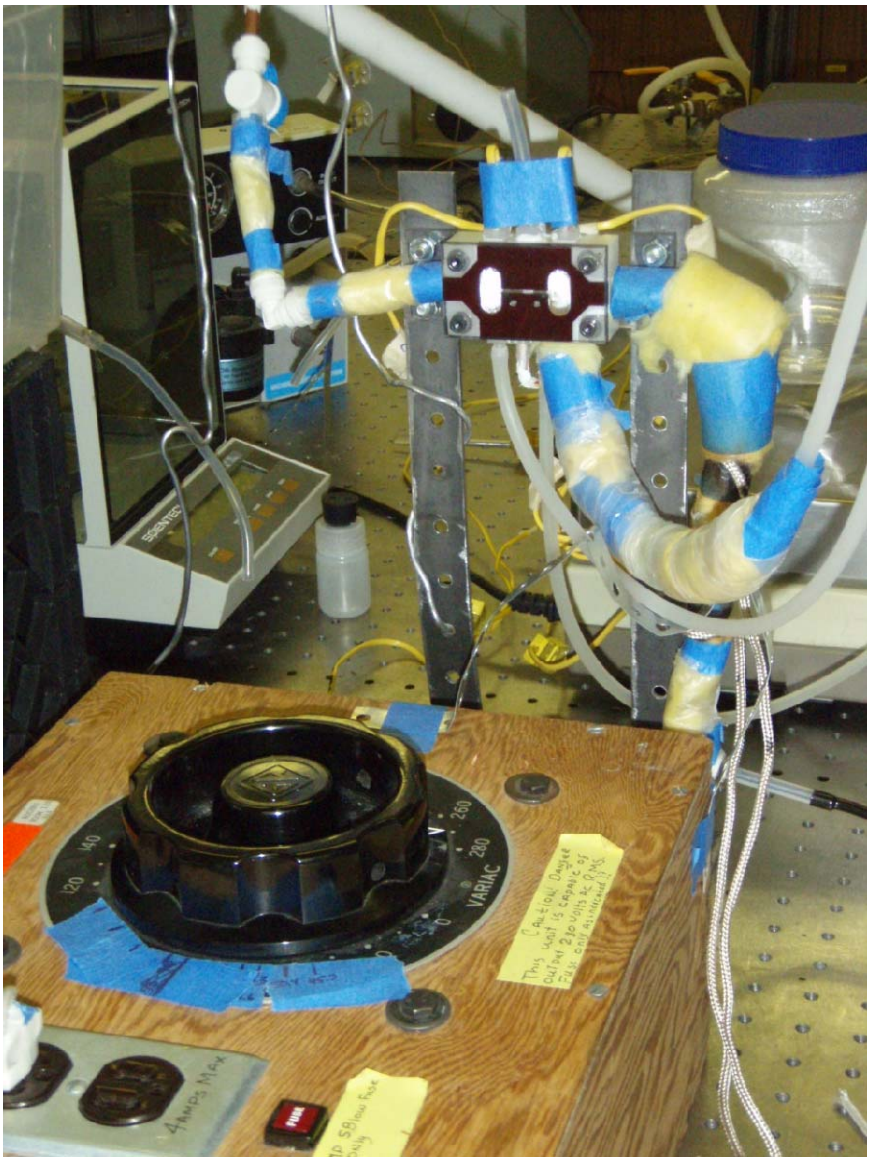

Figure D6: Flow loop

The figure above shows the flow loop from farther back. The black tube entering from the lower right has the inlet flow as set by the syringe pumps not shown (behind the camera taking the picture). The flow passes through a heavily insulated copper tube that has heater tape wrapped around it. The heater tape is the white cord coming out of the insulation and passing out of the bottom of the picture. The cord reenters the picture from the left and plugs into the wooden box. The wooden box is the variac used for controlling the heater tape output. The two tubes coming out of the bottom of the component and towards that camera are the pressure taps to the

inlet and exit plenum. They exit the frame to the right and plug into the differential pressure inclined manometer just outside of the picture. The tube coming out the top of the component is the exit for the extracted vapor. During testing, another tube with insulation and a connection fitting comes down over the tube protruding from the test device. This is how the vacuum is applied. When tube is in place, the vapor is pulled out of the picture to the left and into a condenser. From the condenser, what should be condenser water is now gravity fed into the small plastic bottle shown slightly to the left of middle in the picture. The exiting water-vapor mixture exits the component to the left of the testing device. It then flows into the PVC pipe which acts as the vapor escape chamber, where the water flows down to the mass collector in the background and the vapor comes out the top of the pipe. In this figure, you can again see the thermocouples moving away from the component towards the Data Acquisition Board hidden from view by the water collection container.

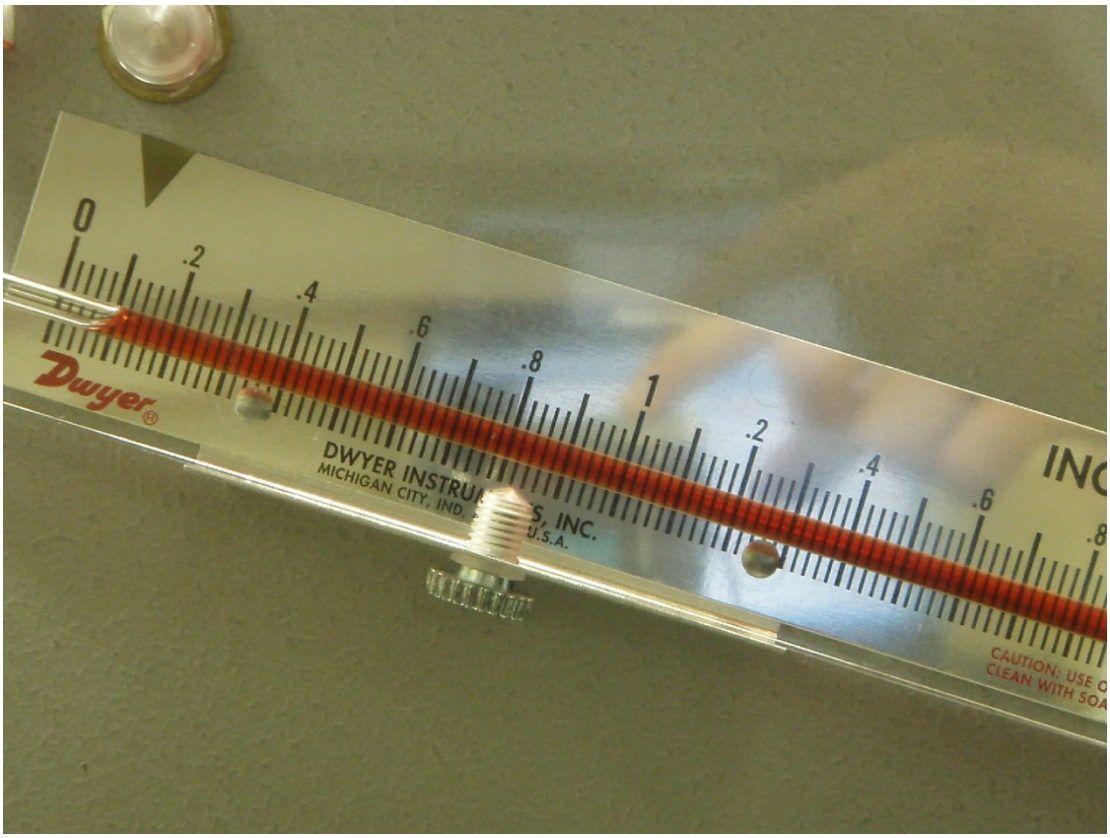

Figure D7: Example single phase pressure drop photo, 5 mL/min flow rate

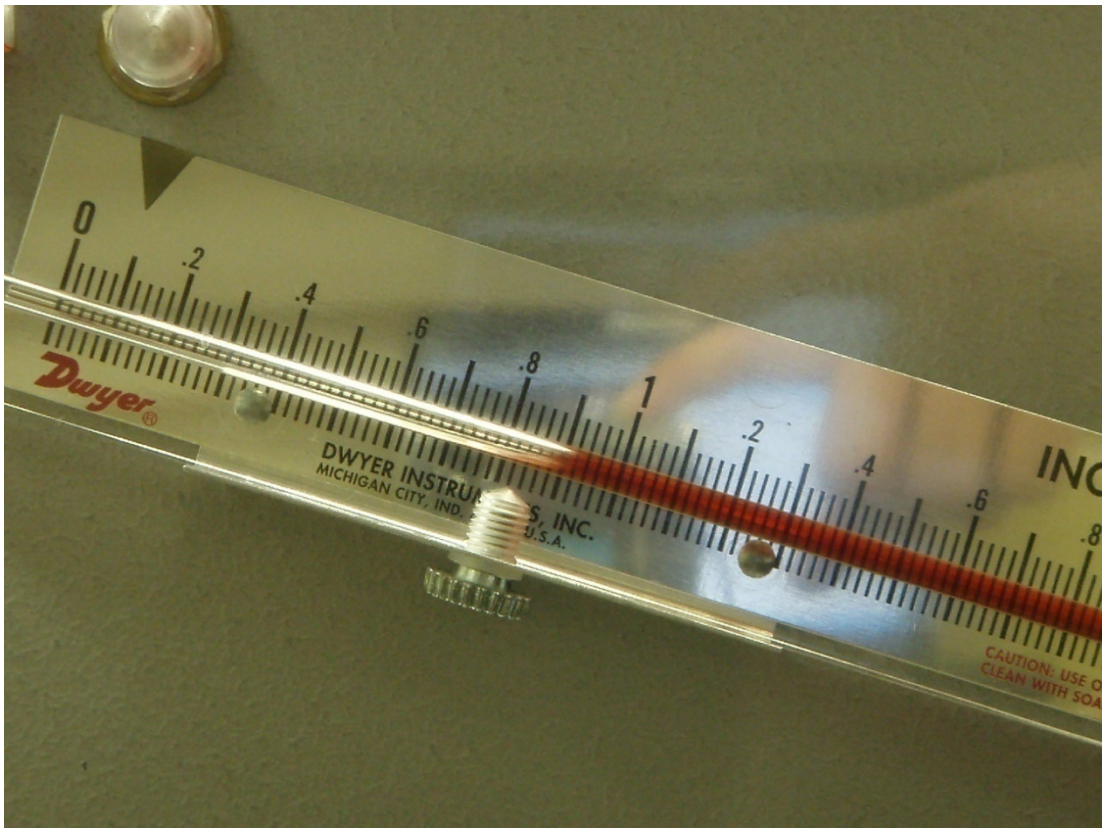

Figure D8: Example two-phase flow pressure drop, 5 mL/min flow rate

The two pictures above are examples of the photos taken by the camera for determining the pressure drop in the channel. The single phase pressure drop was relatively constant, and could have been read by hand, but the two-phase pressure drop changed frequently and with large fluctuations. This difference can actually be seen in the photos shown. The single phase has a more defined level in the manometer because it was stationary with respect to the shutter speed of the camera. It can be seen that the two-phase flow has a less defined level that is due to its rapidly changing level with respect to the camera shutter speed.

Appendix E – NiChrome Heater Deposition Worksheet

The following pages are the spreadsheet used to calculate the sputter deposition times necessary for forming the NiChrome heaters. The power supplied to the target was 100 W. This sputter deposition worksheet is only applicable for Dr. Brady Gibbons sputter deposition machine on the west end of his lab in the spring of 2009. However, the times and data can be used for starting points in the future. Thicknesses and resistances, however, should be applicable for any project.

$R = \frac{\rho l}{wh}$ ---------- ---------- ----------> $h = \frac{\rho l}{wR}$

w =	1.50E-03	m	
l =	2.00E-02	m	
resistivity ρ =	1.30E-06	Ω-m	
(Old Machine)			

	SD Time (s)	Resistance (kΩ)	Resistance (Ω)	Thickness (m)	Thickness (nm)
(Thin leads)	75	80	80000	2.17E-10	0.22
(Thin leads)	150	20	20000	8.67E-10	0.87
(Thick leads)	165	6.4	6400	2.71E-09	2.71
(Thick leads)	210	4	4000	4.33E-09	4.33

$P = V^2 / R$ $\Delta p = \frac{f L \rho v^2}{2 D_h}$

Voltage= 50

$D_h = 4 A / P$ =	0.4344	mm	0.0004344	m
A = H x W =	0.381	mm^2	0.000000381	m^2
P = 2H + 2W =	3.508	mm	0.003508	m
H =	0.254	mm	0.000254	m
W =	1.5	mm	0.0015	m
Density ρ =	971.8	kg/m^3 (80C)		
Source:		http://www.simetric.co.uk/si_water.htm		

L = 20 mm 0.02 m

f = 19.7022 / Re for square duct with aspect ratio 1/6

μ = 3.55E-04 N-s/m^2 (at 80 C)

Source: http://www.engineeringtoolbox.com/water-dynamic-kinematic-viscosity-d_596.html

fRe = 19.6516

Resistance (Ω)	Power (W)
10000	0.250
8000	0.313
6000	0.417
4000	0.625
2000	1.250
1000	2.500
900	2.778
800	3.125
700	3.571
600	4.167
500	5.000
400	6.250

$Re = m D_h / A \mu$

$Q = v A$

Q (ml/min)	(m^3/s)	Re	Δp (Pa)	Δp (psi)	Δp (in H2O)
1	1.67E-08	52.02	16.17	0.002345	0.06492
1.57	2.62E-08	81.75	25.41	0.003685	0.1020
2.14	3.57E-08	111.5	34.65	0.0050255	0.1391
2.71	4.52E-08	141.2	43.89	0.006366	0.1762
3.29	5.48E-08	170.9	53.13	0.007706	0.2133
3.86	6.43E-08	200.7	62.37	0.009046	0.2504
4.43	7.38E-08	230.4	71.61	0.01039	0.2875
5.00	8.33E-08	260.1	80.85	0.01173	0.3246

(all laminar) (all liquid)

Vapor Mass Uncertainty (bias): 0.01 mg

Desired Percent Uncertainty: 0.0100%

Necessary Vapor Extraction: 100 mg 1.00E-04 kg
(This is all assuming no condensation in the tubes)

Inlet Enthalpy 397995 J/kg

Exit Enthalpy (Vapor) 2676000 J/kg

Exit Enthalpy (Liquid) 419000 J/kg

Test with: 4 g/min

M in 6.667E-05 kg/s

Test Time (min)	M v (kg/s)	M l (kg/s)	Power (W)	R	Thickness (nm)
5	3.330E-07	6.633E-05	2.157E+00	1.159E+03	1.500E+01
6	2.770E-07	6.639E-05	2.032E+00	1.231E+03	1.410E+01
7	2.380E-07	6.643E-05	1.942E+00	1.287E+03	1.350E+01
8	2.083E-07	6.646E-05	1.875E+00	1.333E+03	1.300E+01
9	1.851E-07	6.648E-05	1.823E+00	1.372E+03	1.260E+01
10	1.666E-07	6.650E-05	1.781E+00	1.404E+03	1.230E+01
11	1.515E-07	6.652E-05	1.747E+00	1.431E+03	1.210E+01
12	1.388E-07	6.653E-05	1.718E+00	1.455E+03	1.190E+01
13	1.282E-07	6.654E-05	1.694E+00	1.476E+03	1.170E+01
14	1.190E-07	6.655E-05	1.673E+00	1.494E+03	1.160E+01
15	1.111E-07	6.660E-05	1.655E+00	1.510E+03	1.150E+01
16	1.041E-07	6.656E-05	1.640E+00	1.525E+03	1.140E+01

Test with: 5 g/min

M in 8.33333E-05 kg/s

Test Time (min)	M v (kg/s)	M l (kg/s)	Power (W)	R	Thickness (nm)
5.00E+00	3.33E-07	8.30E-05	2.51E+00	9.97E+02	1.74E+01
6.00E+00	2.78E-07	8.31E-05	2.38E+00	1.05E+03	1.65E+01
7.00E+00	2.38E-07	8.31E-05	2.29E+00	1.09E+03	1.59E+01
8.00E+00	2.08E-07	8.31E-05	2.23E+00	1.12E+03	1.54E+01
9.00E+00	1.85E-07	8.31E-05	2.17E+00	1.15E+03	1.51E+01
1.00E+01	1.67E-07	8.32E-05	2.13E+00	1.17E+03	1.48E+01
1.10E+01	1.52E-07	8.32E-05	2.10E+00	1.19E+03	1.45E+01
1.20E+01	1.39E-07	8.32E-05	2.07E+00	1.21E+03	1.43E+01
1.30E+01	1.28E-07	8.32E-05	2.05E+00	1.22E+03	1.42E+01
1.40E+01	1.19E-07	8.32E-05	2.02E+00	1.24E+03	1.40E+01
1.50E+01	1.11E-07	8.32E-05	2.01E+00	1.25E+03	1.39E+01
3.00E+01	5.56E-08	8.33E-05	1.88E+00	1.33E+03	1.30E+01

L w leads= 0.033234 m

SD Time (s)	Resistance (kΩ)	Thickness (m)	Leads?	h (calc) (nm)	h (meas.) profilometer
160	2.1	1.37E-08	Yes	13.72	35.00
160	1.7	1.02E-08	No	10.20	30.00

Correction Factor Needed:

G (Gibbon's Correction factor) $G = \frac{h\ (measured)}{h\ (calculated)}$ Then $h_{actual} = \frac{G\ \rho\ l}{w\ R}$ G = 2.75

(25 mTorr) G included

160	20.4	8.50E-10	No	0.85	2.33
240	1.31	2.20E-08	Yes	21.99	60.40

Slope1: 2.33/160 = 0.0146 nm/s

Slope2: 36.35/240 = 0.2517 nm/s

Average: 0.1331 nm/s

Combined: 0.7258 nm/s Intersect -113.79667

Predictor Method | Time

Slope 1 | 180	30.13	9.558E-10	Yes	0.96	2.63
Slope 2 | 180	1.75	1.649E-08	Yes	16.49	45.30
Average | 180	3.30	8.7230E-09	Yes	8.72	23.96
Combined | 180	4.70	6.1339E-09	Yes	6.13	16.85

SD Time (s)	Resistance (kΩ)	Thickness (m)	Leads?	h (calc)	h (meas.)
180	1.76	1.64E-08	Yes	16.37	44.96
240	1.31	2.20E-08	No	21.99	60.40

Slope1:	44.96/180 =	0.2498	nm/s
Slope2:	36.35/240 =	0.2517	nm/s
Average:	0.2507	nm/s	

Leg Lengths	0.01323 4

Test Piece SD Times (s)	Desired Resistance				
54	3.5	4.95E-09	No	4.95	13.60
190	1	1.73E-08	No	17.33	47.62
2095	0.06	1.91E-07	Legs	191.16	525.12

Sputtered Times

86	3.67	7.85E-09	Yes	7.85	21.56
1800	0.18	1.64E-07	Yes	164.28	451.28

1800	0.07	1.64E-07	Legs	164.28	451.28

Sputter Time	Measured R (kΩ)	Max Power (W)
86 | 1800 legs	5	0.5
1800	0.18	13.89

REFERENCES

Apreotesi, M.A., 2007, "Microscale Thermal Management Utilizing Vapor Extraction from a Fractal-like Branching Heat Sink", Oregon State University, Corvallis, OR.

Beavers, G.S. and Joseph, D.D., 1967, "Boundary Conditions at a Naturally Permeable Wall, J. Fluid, Mech., **30**, pp 197-207.

Chellam, S., Weisner, M.R. and Dawson, C., 1992, "Slip at a Uniformly Porous Boundary: effect on Fluid Flow and Mass Transfer", J. Engr Math., **26**, pp 481-492.

Jiang, L., M. Wong, M. and Y. Zohar, Y., "Forced Convection Boiling in a Microchannel Heat Sink", Journal of Microelectromechanical Systems, **10**, pp. 80-87, 2001.

Lawson, K.M. and Lloyd, D.R., 1997, "Membrane distillation", J. Membrane Science, 1997. **124**(1), p. 1-25.

Mason, E.A. and Malinauskas, A.P., 1983, *Gas transport in porous media: the dusty-gas model*, Elsevier Scientific Pub. Co. Amsterdam.

Mertz, R., A. Wein, A., and M. Groll, M., "Experimental investigation of flow boiling heat transfer in narrow channels", Second European Thermal Sciences and 14th UIT National Heat Transfer Conference, Rome, 1996.

Qu, W. and I. Mudawar, I., "Experimental and numerical study of pressure drop and heat transfer in a single-phase micro-channel heat sink", International Journal of Heat and Mass Transfer, **45**, pp. 2549-2565, 2002.

Qu, W. and Mudawar, I., W. Qu and I. Mudawar, "Measurement and prediction of pressure drop in two-phase micro-channel heat sinks", International Journal of Heat and Mass Transfer, **46**, pp. 2737-2753, 2003.

Qu, W. and I. Mudawar, "Transport phenomena in two-phase micro-channel heat sinks." Journal of Electronic Packaging, Transactions of the ASME, **126**, p. 213-224, 2004.

Saffman, P.G., 1971, "On the Boundary Condition at the Surface of a Porous Medium", Studies in Applied Math., **L**(2), pp 93-101.

Salakij, S., Liburdy, J.A. and Pence, D.V., 2009, "Modeling In-Situ Vapor Extraction During Convective Boiling", accepted ASME FEDSM 2009, Vail CO.

Sarti, G.C., Gostoli, C., and Bandini, S., 1993, "Extraction of Organic Components from Aqueous Streams by Vacuum Membrane Distillation", J. Membrane Science, **80**(1) p. 21-33.

Schofield, R.W., Fane, A.G., and Fell, C.J.D., 1987, "Heat and Mass Transfer in Membrane Distillation", J. Membrane Science, **33**, p. 299-313.

Shaw, R.K. and London, A.L., 1978, *Laminar Flow Forced Convection in Ducts*, Academic Press, New York, pp. 196-221, Chap. 7.

Smolders, C.A. and Franken, A.C.M., 1989, "Terminology for membrane distillation", Desalination, 1989. **72**, p. 249-262.

Steinke, M. E., and Kandlikar, S. G., "An Experimental Investigation of Flow Boiling Characteristics of Water in Parallel Microchannels", Journal of Heat Transfer, **126**, pp. 518-526, 2004.

Tomaszewska, M., 1999, "Membrane Distillation", Environment Protection Engineering, 1999. **25**, p. 37-47.

Trethway, D.C. and Meinhart, C.D, 2002, "Apparent Fluid Slip at Hydrophobic Microchannel Walls", Physics of Fluids, **14**(3), pp L9-L12.

Tuckerman, D. B. and Pease, R. F. W., "High-Performance Heat Sinking for VLSI, IEEE Electron Device Lett.", **EDL**(2), pp. 126-129, 1981.

Vinayak, S., Srivastav, R.D., Sehgal, B.K., Naik, A.A., Prabhakar, S., Guru, V., Saravanan, S., Mahajan, S., Agarwal, V.R., Gulati, R., Vyas, H.P., 2002, "Development and TCR control of Nichrome thin film resistors for GaAs MMICs" Proceedings of SPIE - The International Society for Optical Engineering, **4746** (II), pp. 936-939.

White, F.M., 2008, *Fluid Mechanics*, McGraw Hill, Boston, pp. 346-350, Chap. 6

Zhang, L., Banerjee, S. S., J. Koo, J., D.J. Laser, D.J., M. Ashegi, M., K.E. Goodson, K.E., Santiago, J. G., and T.W. Kenny, T.W., "A micro heat exchanger with integrated heaters and thermometers", Proceedings of Solid State Sensor and Actuator Workshop, pp. 275-280, 2000.

Zhang, L., J. Koo, J., L. Jiang, L., M. Ashegi, M., Goodson, K. E., Santiago, J. G., and T.W. Kenny, T.W., "Measurement and Modeling of Two-Phase Flow in Microchannels with Nearly Constant Heat Flux Boundary Conditions", Journal of Microelectromechanical Systems, **11**, pp. 12-19, 2002.

Zhou, P., Goodson, K., and Santiago, J., 2006, US Patent No. 6,994,151. Washington, DC: US Patent and Trademark Office. Retrieved October 19, 2008 from: http://www.google.com/patents?id=IdV2AAAAEBAJ